ORIGINAL PAPER

Probabilistic urban cascading multi-hazard risk assessment methodology for ground shaking and post-earthquake fires

Tomoaki Nishino[1] ©

© The Author(s) 2023

Abstract

A probabilistic methodology is presented for assessing cascading multi-hazard risk for ground shaking and post-earthquake fires at a regional scale. The proposed methodology focuses on direct economic losses to buildings caused by the combined effect of ground shaking and post-earthquake fires and evaluates the exceedance probability of the regional shaking–fire losses in a predefined future time period by comprehensively considering the effects of various uncertain factors on the losses via Monte Carlo simulations. Probabilistic seismic risk assessments are extended by integrating post-earthquake fire models with seismic activity models, ground motion prediction equations, and seismic fragility functions. The fire models include post-earthquake ignition models, a weather model, a physics-based urban fire spread model, and a fire brigade response model. This integrated modeling enables the incorporation of the following uncertain factors with causal relationships into the assessments: earthquake occurrence, ground motion intensity distribution, damage to buildings resulting from ground shaking, post-earthquake ignition occurrence and occupant firefighting, weather condition, fire brigade response time including time to detection, and damage to buildings resulting from post-earthquake urban fire spread. To demonstrate the methodology, a realistic case study is conducted for a historical urban area with closely spaced wooden buildings in Kyoto, Japan, focusing on possible large earthquakes along major active faults. Contrary to conventional single-hazard approaches, the results highlight the impact of multi-hazard consideration on risk assessments. This indicates that the methodology can be a useful tool for more appropriately understanding earthquake risk and promoting risk-informed decision-making in urban communities for risk reduction.

Keywords Multi-hazard risk assessment · Seismic damage · Fire following earthquake · Urban fire spread · Probabilistic loss estimation · Epistemic uncertainty

✉ Tomoaki Nishino
    nishino.tomoaki.3c@kyoto-u.ac.jp

1   Disaster Prevention Research Institute, Kyoto University, Gokasho, Uji, Kyoto 611-0011, Japan

1 Introduction

Urban settlements congested with flammable wooden buildings are at risk from cascading earthquake hazards of not only ground shaking but also fires. Once fires start in such areas, they easily spread to adjacent buildings as a result of the narrow distance between buildings. Post-earthquake fires can therefore have a significant impact on communities, in addition to other secondary hazards, including liquefaction, landslides, and tsunamis. Historically, large earthquakes hitting urban areas have triggered simultaneous outbreaks of multiple fires; some such fires have developed into spreading fires, resulting in significant losses to society (Scawthorn 1986; Scawthorn et al. 1996, 2006). For example, the Great Fire of Tokyo after the Kanto earthquake, which had a magnitude of 7.9 and struck the Tokyo-Yokohama metropolitan area, Japan, on September 1, 1923 (11:58 a.m. local time), was the most devastating post-earthquake fire in history, destroying over 220,000 buildings and killing over 55,000 people (Ogata 1925). This devastating damage occurred because (1) the earthquake occurred when numerous fires were being used for cooking, (2) the urban area had a high density of flammable wooden buildings, and (3) a strong wind faster than 10 m/s was blowing at the time of the event. A study by Nishino et al. (2013) suggested that wind-blown fire plumes could have covered a broad area of Tokyo and therefore had a significant adverse impact on urban fire evacuation by exposing evacuees to hot and toxic gases, resulting in enormous human damage. Various measures have subsequently been implemented in Japan to improve the fire resistance of urban settlements, and consequently, conflagrations have become rare events. The Kobe earthquake, however, which had a magnitude of 7.3 and struck Kobe, Japan, and its surrounding area on January 17, 1995 (5:46 a.m. local time), demonstrated that the risk of post-earthquake fires still exists in modern cities in Japan. As many as 269 fires were ignited after the earthquake, and some of these fires developed into conflagrations, resulting in over 7000 buildings being burned despite the early-morning occurrence of the earthquake and the calm weather (Fire Disaster Management Agency 2006). Sekizawa (1998) reported that the number of fire engines dispatched per fire was critical to whether the fire brigades successfully controlled the simultaneous fires following the Kobe earthquake. Because the risk of post-earthquake fires is also being seriously considered in other earthquake-prone countries (Coar et al. 2021; Lee et al. 2008; Thomas et al. 2012), such as the USA and New Zealand, an integrated earthquake risk management system including post-earthquake fires is a universal challenge in forming earthquake-resilient communities that several countries are facing. To manage this risk, it is important to understand the variability of potential consequences resulting from cascading multi-hazards at the regional scale by considering differences in the regional damage-causing mechanisms between ground shaking and post-earthquake fires. For example, post-earthquake fires will eventually cause damage to buildings that are widely distributed throughout a region. This is similar to the effect of ground shaking. However, the damage propagation of fires has spatial and temporal dependences, such as the distance between buildings and temporal changes in the wind velocity and direction; this differs from the effect of ground shaking, to which widely distributed buildings are almost simultaneously subjected. In addition, the regional damage caused by post-earthquake fires increases with the earthquake magnitude similar to the regional damage caused by ground shaking because the potential of fire outbreaks is strongly correlated with the strength of the ground shaking (Davidson 2009; Khorasani et al. 2017; Nishino and Hokugo 2020).

Because many areas of the world are liable to suffer from multiple natural hazards, a number of studies have proposed multi-hazard risk analysis approaches to identify effective

risk reduction policies and strategies that consider all of the relevant threats in a region (Cousins et al. 2012; Goda and Risi 2018; Goda et al. 2021; Kappes et al. 2012; Marzocchi et al. 2012; Mignan et al. 2014; Ming et al. 2015; Omidvar and Kivi 2016; Schmidt et al. 2011; Selva 2013). Most of these approaches integrate existing methodologies for hazard modeling and risk assessment and estimate the overall hazard and risk levels in addition to comparing the individual risk levels under homogeneous risk definitions and considering all possible risk interactions. Conversely, post-earthquake fire risk analyses (e.g., Baquedano Julia et al. 2021; Coar et al. 2021; Nishino et al. 2012; Scawthorn 2011) have generally focused on regional fire losses alone without considering possible combined losses resulting from ground shaking and post-earthquake fires, even though most analyses have considered the effects of seismic damage to structures and water pipelines on regional fire damage. Regional combined loss estimations for ground shaking and post-earthquake fires can be useful in cost–benefit analyses of various risk reduction measures for single- or multi-hazard scenarios. For example, joint or collaborative rebuilding, where people cooperate in rebuilding by pooling and adjusting their individual properties or property rights, is an effective risk reduction option typically used in Japan to improve the resistance of urban areas consisting of many closely spaced wooden buildings against both ground shaking and post-earthquake fires, even though this approach typically requires large amounts of time and effort and may impair historical streetscapes. Conversely, seismic or fire retrofitting, which is individually conducted by building owners, can be a risk reduction option for either ground shaking or post-earthquake fires. In addition, seismic circuit breakers for household use, which are activated after being subjected to shaking exceeding a certain level and cut the power supply to prevent ignition from electrical appliances and wirings, have recently been recommended as a low-cost, fast risk reduction option for post-earthquake fires given that most instances of fire ignition in buildings after recent major earthquakes resulted from electricity-related sources (Nishino and Hokugo 2020). Promoting risk-informed decision-making is important to enable communities to reasonably select risk reduction options, and a cascading multi-hazard risk assessment for ground shaking and post-earthquake fires can play a critical role in this context. Nevertheless, with the exception of Cousins et al. (2012), much less work has been done to develop a methodology for cascading shaking–fire risk assessments, even though probabilistic modeling for regional losses resulting from ground shaking alone has been well established (e.g., Dolce et al. 2021; Goda and Hong 2008; Kalakonas et al. 2020).

Cousins et al. (2012) extended a regional seismic loss estimation methodology to include post-earthquake fire losses and probabilistically determined the significance of post-earthquake fires for a city with many closely spaced wooden buildings. Their methodology was based on a static urban fire model that describes the eventual extent of fire damage by assuming that the building-to-building distance critical to stop the fire spread depends on the wind velocity; accordingly, the wind velocity was treated as the only uncertain factor associated with the fire loss estimations. However, the behavior of urban fire spread greatly depends on the wind direction and fires typically spread much faster in the downwind direction. Because the time variations in both the wind velocity and the wind direction, combined with the irregularity of the spatial distribution of the buildings, produce the complex behavior of an urban fire spread, a static model independent of the wind direction cannot capture realistic fire spread behavior. In particular, a static model that deterministically specifies the distance limit for building-to-building fire spread neglects the possible occurrence of spot fires resulting from firebrands, which are important urban fire spread mechanisms, in addition to window-ejected flame radiation and wind-blown fire plume convection. Therefore, a static model is likely to result in fire loss underestimations,

which are undesirable for disaster risk management. Numerous firebrands originating from burning buildings can travel long distances on the wind and fall on downwind buildings. Some of these firebrands can ignite combustible objects in or around buildings distant from burning buildings; therefore, spot fires resulting from firebrands have a probabilistic aspect. To more appropriately estimate fire losses, which influence combined shaking–fire losses, a new cascading shaking–fire risk assessment methodology needs to be developed that includes a physics-based dynamic fire loss model that is capable of capturing urban fire spread mechanisms. Several studies (Himoto and Tanaka 2008; Lee and Davidson 2010; Nishino 2019; Zhao 2010) have developed physics-based urban fire spread models. In particular, Nishino (2019) incorporated a stochastic model for the occurrence of spot fires resulting from firebrands into a physics-based model that treats window-ejected flame radiation and wind-blown fire plume convection as urban fire spread mechanisms; the model performance was validated by numerically reproducing the 2016 Itoigawa Great Fire, which was the most recent conflagration under strong wind conditions in Japan to cause devastating damage to urban settlements composed of old wooden buildings. Adopting such a physics-based dynamic model also has the advantage of being able to comprehensively consider various uncertainties associated with the behavior of urban fire spread. For example, Nishino et al. (2012) proposed a methodology to assess the variability of post-earthquake fire losses via Monte Carlo simulations based on a physics-based urban fire spread model. Their methodology treats uncertain factors associated with the behavior of urban post-earthquake fire spread via the following inputs: the number and locations of fire outbreaks, weather (outdoor air temperature and wind velocity and direction), and structural damage resulting from ground shaking (i.e., differences in the fire behavior between collapsed and non-collapsed buildings). In addition, such a physics-based dynamic model makes it possible to physically reflect the effect of fire brigade firefighting on fire loss estimations and to consider uncertainty in firefighting. For example, fire detection by fire brigades tends to be delayed during earthquake events compared with normal times because calls to fire brigades are typically jammed after earthquakes as a result of the many non-emergency calls unrelated to the earthquake, fires, and rescues (Sugii et al. 2008). Therefore, the time to detection after earthquakes, which has a much greater level of variation than that during normal times, can be an important uncertain factor that influences fire loss estimations.

The present study develops a novel probabilistic methodology for assessing the cascading multi-hazard risk for ground shaking and post-earthquake fires at a regional scale. The proposed methodology focuses on direct economic losses to buildings caused by the combined effect of ground shaking and post-earthquake fires and evaluates the exceedance probability of the regional shaking–fire losses in a predefined future time period by comprehensively considering various uncertainties via Monte Carlo simulations. The methodology is an extension of a typical probabilistic seismic risk assessment and is built on national seismic activity models for Japan (Morikawa and Fujiwara 2016), which include earthquakes both with and without specified source faults across Japan. The methodology focuses on earthquakes with specified source faults, such as major active faults, because their magnitude and occurrence probability can be evaluated from historical records and geological and geographical data. Note that the methodology is developed for buildings in Japan; however, the methodology is flexible and can be changed depending on the given requirements. To quantitatively evaluate the combined losses to buildings as a result of ground shaking and post-earthquake fires, post-earthquake fire damage prediction models are integrated with ground motion prediction equations and seismic fragility functions and replacement costs are then introduced to convert the predicted damage into losses. The post-earthquake fire damage prediction models include the following:

(1) empirical post-earthquake ignition prediction equations that describe the ignition probability per exposure population as a function of the ground motion intensity, (2) an empirical weather model that randomly extracts time history samples for a given time period from hourly recorded weather data for outdoor air temperature and wind velocity and direction, (3) a physics-based dynamic urban fire spread model that describes the time-varying behavior of individual building fires by considering the building-to-building fire spread mechanisms, and (4) a fire brigade response model that automatically specifies water spray targets depending on the simulated fire spread situations on the basis of the predefined decision-making rules of the fire brigades. The post-earthquake ignition prediction equations are developed here by statistically analyzing the fire records for several past major large earthquakes in Japan. The equations, which are Poisson regression models, are derived individually for each earthquake following previously reported approaches (Nishino and Hokugo 2020; Nishino 2021) to consider the effects of the differences in the regression models depending on the earthquake on the risk estimates. The urban fire spread model is extended here by incorporating the effects of structural damage resulting from ground shaking and water spray by firefighters into the existing physics-based model (Nishino 2019) to simulate realistic urban fire spreading behavior following an earthquake. The fire brigade response model is further developed by dividing the response process into several stages of fire detection, travel to water sources, hose extension, and water spray. The decision-making rules of the fire brigades are defined to describe a realistic placement of the fire engines with respect to the water sources and a realistic selection of targets for water spray considering that firefighting in large urban fires focuses on preventing the spread of fires to neighboring unburned buildings rather than extinguishing burning buildings and preferentially arranges fire hose nozzles in highly likely fire spread directions. The time to complete the hose extension is modeled considering the high uncertainty in the time to fire detection, and its statistical distributions are developed by analyzing the fire records for several past major large earthquakes in Japan. The proposed methodology is demonstrated via a realistic case study for a historical urban area with closely spaced wooden buildings in Kyoto, Japan, focusing on possible large earthquakes along major inland active faults. The case study provides an illustration of a multi-hazard risk assessment in contrast with single-hazard risk assessments. The case study also investigates how much the shaking–fire risk estimates vary depending on which model to select from seismic fragility models (functions) or post-earthquake ignition models (prediction equations), which is a key issue in practical application. Note that this sensitivity analysis is limited to these models considered particularly important because there are dependencies among some models and it may be difficult to systematically investigate the contribution to the risk for all models.

The paper is organized as follows. Section 2 formulates the multi-hazard risk for ground shaking and post-earthquake fires and presents the computational framework and implemented models. Section 3 illustrates the application of the proposed methodology and presents a discussion of the impact of multi-hazard considerations on risk assessments. Finally, Sect. 4 presents the study conclusions and potential future work.

2 Proposed methodology

2.1 Risk formulation

The cascading multi-hazard risk for ground shaking and post-earthquake fires follows the general definition of seismic risk, which is represented as the relationship between a given

loss and its exceedance probability in a predefined future time period when all possible earthquakes are considered. The proposed methodology focuses on direct economic losses to buildings at the regional scale caused by the combined effect of ground shaking and post-earthquake fires. The risk is therefore defined as the probability $p(L \geq l;t)$ that the total loss L to the buildings caused by the combined effect of ground shaking and post-earthquake fires exceeds a certain threshold l at least once within t years when all possible earthquakes are considered:

$$p(L \geq l;t) = 1 - \prod_k \left[1 - p_k(L \geq l;t)\right], \tag{1}$$

where $p_k(L \geq l;t)$ is the probability that the total loss L exceeds a certain threshold l at least once within t years when the k-th earthquake is considered.

Assuming that the probability of earthquakes occurring more than once within t years is negligible, the probability $p_k(L \geq l;t)$ can be given as

$$p_k(L \geq l;t) = p\left(E_k;t\right)p\left(L \geq l\middle|E_k\right), \tag{2}$$

where $p\left(E_k;t\right)$ is the probability that the k-th earthquake occurs within t years and $p\left(L \geq l\middle|E_k\right)$ is the probability that the total loss L exceeds a certain threshold l when the k-th earthquake occurs.

While the earthquake occurrence probability $p\left(E_k;t\right)$ can be evaluated using country-specific seismic activity models (e.g., Morikawa and Fujiwara 2016), the conditional loss exceedance probability $p\left(L \geq l\middle|E_k\right)$ needs to be numerically evaluated via Monte Carlo simulations, which stochastically generate numerous realizations. Hence, the probability $p\left(L \geq l\middle|E_k\right)$ can be given as

$$p\left(L \geq l\middle|E_k\right) = \frac{1}{n_{MCS}} \sum_{j=1}^{n_{MCS}} I\left(L_j \geq l\middle|E_k\right), \tag{3}$$

where n_{MCS} is the number of Monte Carlo trials and $I(\cdot)$ is the indicator function that takes a value of 1 when the total loss for the j-th trial L_j is greater than or equal to l and takes a value of 0 otherwise.

The total loss for the j-th trial L_j can be written as

$$L_j = \sum_{i=1}^{n_{bldg}} L_{ij} = \sum_{i=1}^{n_{bldg}} \max\left(L_{S,ij}, L_{F,ij}\right), \tag{4}$$

where n_{bldg} is the number of buildings and L_{ij}, $L_{S,ij}$, and $L_{F,ij}$ are the losses resulting from the combined effect of ground shaking and post-earthquake fires, only ground shaking, and only post-earthquake fires, respectively, for the i-th building and the j-th trial. Note that the above equation is applicable when ground shaking and post-earthquake fires can be assumed to dominantly contribute to the losses to buildings.

Introducing the total replacement cost of the i-th building $C_{R,i}$ and the loss ratios for ground shaking and post-earthquake fires, $LR_{S,ij}$ and $LR_{F,ij}$, respectively, for the i-th building and the j-th trial, Eq. (4) can be expressed as

$$L_j = \sum_{i=1}^{n_{bldg}} \left[C_{R,i} \times \max\left(LR_{S,ij}, LR_{F,ij}\right)\right]. \tag{5}$$

The total replacement cost $C_{R,i}$ can be determined by multiplying the total floor area by the unit replacement cost (i.e., the replacement cost per floor area), which can be obtained from building statistics depending on the construction type. The loss ratio for ground shaking $LR_{S,ij}$ is determined depending on the damage state, which can be evaluated using seismic fragility functions. Meanwhile, the loss ratio for post-earthquake fires $LR_{F,ij}$ is defined as the ratio of the number of fire-involved rooms to the total number of rooms, which can be evaluated using a physics-based urban fire spread model.

2.2 Computational framework and implemented models

Figure 1 illustrates the computational framework for assessing the cascading multi-hazard risk for ground shaking and post-earthquake fires formulated in Sect. 2.1. The framework incorporates the following uncertain factors influencing the regional shaking–fire losses into the assessments: (a) earthquake occurrence, (b) ground motion intensity distribution, (c) damage to buildings resulting from ground shaking, (d) post-earthquake ignition occurrence and occupant firefighting during the initial stages, (e) weather condition (here outdoor air temperature and wind velocity and direction are considered), (f) fire brigade response time including time to detection, and (g) damage to buildings resulting from post-earthquake urban fire spread. Note that there are causal relationships between the uncertain factors as indicated by arrows in Fig. 1. For example, the post-earthquake ignition occurrence is directly correlated with the ground motion intensity distribution; therefore, the ground motion intensity distribution indirectly affects the damage to buildings resulting from post-earthquake urban fire spread, which directly depends on factors (d)–(f). In addition, the damage to buildings resulting from ground shaking can enhance building-to-building fire spread and change the burning behavior of buildings themselves, thus influencing the damage to buildings resulting from post-earthquake urban fire spread. While the earthquake occurrence probability is provided by national seismic activity models for Japan (Morikawa and Fujiwara 2016) together with fault location and geometry and earthquake magnitude, the effects of the other uncertain factors are considered in evaluating the conditional shaking–fire loss exceedance probability via Monte Carlo simulations [i.e., Eq. (3)], where a series of simulations of ground shaking, seismic damage, and post-earthquake urban fire spread is implemented for stochastically generated numerous scenarios. The framework is therefore composed of four main modules: (1) seismic activity setup, (2) ground shaking simulation and seismic damage prediction, (3) post-earthquake fire damage prediction, and (4) loss exceedance curve development. While the ground shaking simulation and seismic damage prediction are based on empirical models that evaluate the ground motion intensity and damage state of buildings without dynamically simulating seismic wave propagation and seismic response of buildings, the post-earthquake fire damage prediction is a dynamic assessment based on a physics-based model that describes the time-varying behavior of post-earthquake urban fire spread and predicts physical quantities for fires as a function of time. However, the losses resulting from post-earthquake fires are determined using the eventual damage to buildings resulting from them. This series of assessments is a one-way coupling simulation where the ground shaking and seismic damage influence the behavior of post-earthquake urban fire spread, while the fire has no influence on the ground shaking and seismic damage. Note that the detailed data on the spatially distributed buildings are used as exposure that contain information concerning the building footprints, floors, and construction types, in addition to the position coordinates of the buildings. Such detailed
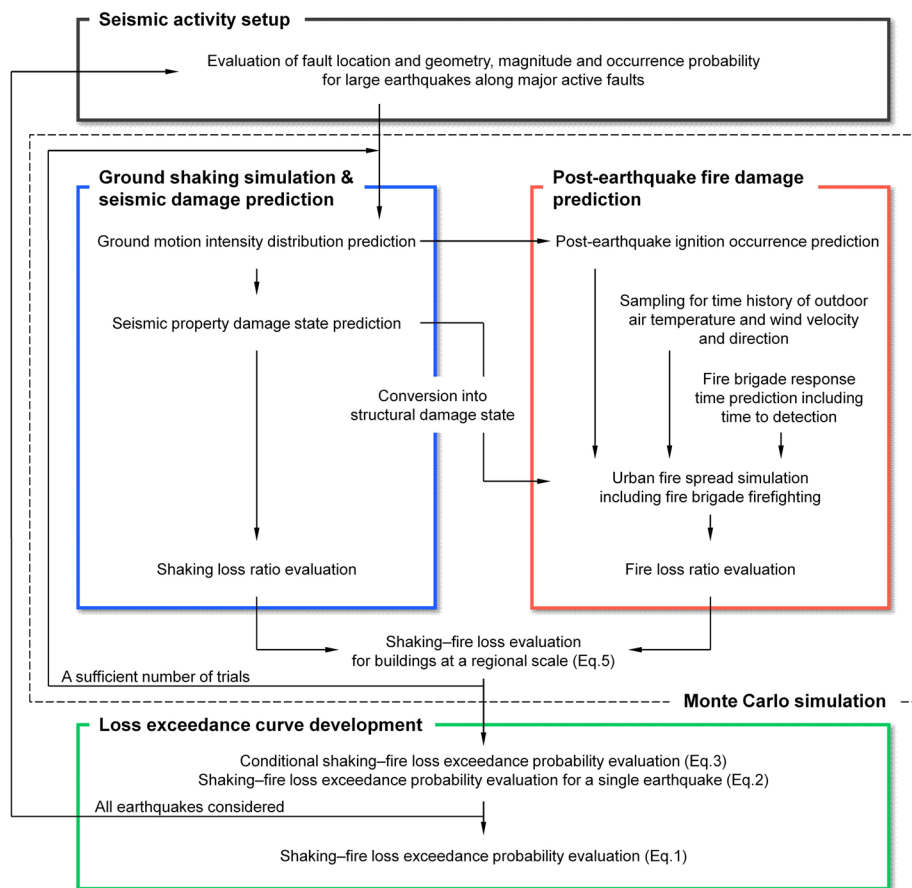
Fig. 1 Computational framework for assessing the cascading multi-hazard risk for ground shaking and post-earthquake fires at a regional scale

building exposure data are required for post-earthquake fire damage prediction, as opposed to seismic damage prediction.

The fault location and geometry, magnitude, and occurrence probability are set for large earthquakes with the specified source faults (here, earthquakes along major active faults) using national seismic activity models for Japan (Morikawa and Fujiwara 2016), which are based on a long-term evaluation conducted by the Earthquake Research Committee of Japan. To obtain the spatial distribution of the ground motion intensities, ground shaking simulations are performed using an empirical ground motion prediction equation, which is a regression model based on strong ground motion records. Here, the seismic source, propagation path, and site effects on the ground motion intensities are expressed as a relatively simple equation because theoretical or semi-empirical approaches take too much time and effort to simulate the various scenarios required for the probabilistic risk assessments. The obtained ground motion intensity distribution is used to evaluate not only the seismic damage probability but also the post-earthquake ignition probability for individual buildings. The Japan Meteorological Agency (JMA)

seismic intensity is adopted as the intensity measure in this study. This intensity measure has no physical unit, unlike acceleration and velocity, but is used here because (1) the JMA seismic intensity is one of the intensity measures commonly used in Japan, (2) it is typically calculated from three-component acceleration waveforms by applying specific filters such that it can emphasize a period range influential to damage to low-rise and mid-rise buildings, damage to goods and equipment inside buildings, and body sensations of shaking (Sakai and Koyama 2016), and (3) it can be predicted using empirical ground motion prediction equations in the same manner as other intensity measures such as the peak ground acceleration and velocity. The property damage states resulting from ground shaking are evaluated for individual buildings considering the differences in the empirical seismic fragility functions depending on the earthquake. The property damage states considered are completely destroyed and half-destroyed, and their corresponding loss ratios to the total replacement cost are assigned accordingly.

The post-earthquake fire damage prediction module first evaluates the post-earthquake ignition incidents, weather, and fire brigade response time and then performs urban fire spread simulations treating these variables as inputs. To determine the origin buildings of the fires, the post-earthquake ignition probability is evaluated for individual buildings considering the differences in the empirical post-earthquake ignition prediction equations depending on the earthquake; then, the probability of an ignition incident inside a building developing into a fire involving the entire building is evaluated considering the occupant firefighting probability during the initial stages. Time histories of the outdoor air temperature and the wind velocity and direction are randomly sampled for a given time period from hourly recorded weather data. The fire brigade response time, including the time to detection, is evaluated for individual fire outbreaks by stochastically generating the time to detection from its statistical distribution and deterministically evaluating the travel time to water sources and the time required for hose extension. Note that only fire cisterns are treated as water sources available for fire brigade firefighting because fire hydrants are less likely to be available following large earthquakes as a result of seismic damage to water pipelines (e.g., Gehl et al. 2021); that is, the post-earthquake availability of fire hydrants is neglected. This aspect of the modeling needs to be improved in future work. To evaluate the post-earthquake fire loss ratio to the total replacement cost for individual buildings, urban fire spread simulations are performed using a physics-based dynamic urban fire spread model including fire brigade firefighting, for which targets are automatically specified depending on the simulated fire spread situations on the basis of predefined decision-making rules for the fire brigades. Note that structural damage resulting from ground shaking influences the behavior of the urban fire spread; therefore, these influences are modeled depending on the structural damage states. For example, if the exterior wall mortar falls off, exposing exterior wall wooden members, this will enhance the building-to-building fire spread. The structural damage states considered are collapsed, heavily damaged, and moderately damaged; these states are assigned to individual buildings considering their statistical correlation with the pre-evaluated property damage states (Miyakoshi et al. 2000).

More details concerning the implemented models are described in the following subsections; however, the framework illustrated in Fig. 1 is flexible and the implemented models can be replaced or improved depending on the given requirements. Note that epistemic uncertainty, which is known to be the uncertainty of the model due to a lack of knowledge and is often characterized by alternative models (e.g., Matsushima 2020), is not fully discussed here, except for the seismic fragility functions and the post-earthquake ignition prediction equations. This aspect needs to be further considered in future work.

2.2.1 Seismic activity model

Seismic activity, which is important information for the probabilistic risk assessment, is modeled for earthquakes with specified source faults. Because the proposed methodology is developed for buildings in Japan, the fault location and geometry, earthquake magnitude, and occurrence probability can be determined using national seismic activity models for Japan (Morikawa and Fujiwara 2016) developed for nationwide probabilistic seismic hazard mapping. These models include more than 200 active faults in Japan, and their detailed model parameters are derived from a long-term evaluation conducted by the Earthquake Research Committee of Japan based on historical records and geological and geographical data. The JMA magnitude can be evaluated based on the entire fault length and can be converted into the moment magnitude in accordance with the strong ground motion prediction method for earthquakes with specified source faults provided by the Earthquake Research Committee of Japan (2017), called the "Recipe." The earthquake occurrence probability can be evaluated using a Brownian passage time model (Ellsworth et al. 1999; Matthews et al. 2002), which is a physically motivated model for earthquake recurrence based on the Brownian relaxation oscillator and assumes that intervals between earthquake events follow a Brownian passage time distribution parameterized by the mean recurrence interval and the aperiodicity of the mean. In a case in which the time of the latest event is unknown, the earthquake occurrence probability can be evaluated using a homogeneous Poisson process model.

2.2.2 Ground motion intensity model

The ground motion intensity measures at the building locations are stochastically evaluated using an empirical ground motion prediction equation. This is a regression model based on the strong ground motion records that simply formulates the seismic source, propagation path, and site effects on the intensity measures, including the probabilistic prediction error quantification. The JMA seismic intensity I_{JMA} is adopted as the intensity measure because not only existing seismic fragility functions (e.g., Midorikawa et al. 2011; Wu et al. 2016; Yamaguchi and Yamazaki 2001) but also existing post-earthquake ignition prediction equations (e.g., Nishino and Hokugo 2020; Nishino 2021) adopt this parameter as an explanatory variable, in addition to the reasons detailed in Sect. 2.2. The ground motion prediction equation developed by Morikawa and Fujiwara (2013) was selected from the existing equations because (1) it is an up-to-date model for Japan based on recorded strong ground motion data up to the end of 2011, (2) the records included in the data range from 5.5 to 9.0 for the moment magnitude and from 1 to 200 km for the source-to-site distance, making it applicable to near-fault sites, as discussed in Sect. 3, as well as large earthquakes, and (3) it can predict the JMA seismic intensity. This equation describes the mean value of the JMA seismic intensity at a site for a given scenario as a function of the moment magnitude M_w and the shortest distance from the fault plane X assuming that the prediction error ε follows a normal distribution with a mean of zero and a standard deviation of σ. The regression coefficients of the equation were obtained for each type of earthquake, e.g., for crustal earthquake types,

$$\frac{I_{JMA}}{2} = -0.0321\left(M'_{w1} - 16.0\right)^2 - 0.003736X + 6.9301$$
$$- \log_{10}\left(X + 0.005078 \times 10^{0.5M'_{w1}}\right) + G_d + G_s + \varepsilon,$$

$$(6)$$

$$M'_{w1} = \min\left(M_w, 8.2\right).$$

$$(7)$$

This equation includes additional correction terms, G_d and G_s, for site amplification as a result of deep sedimentary layers and shallow soft soils, respectively. These additional correction terms, which reduce the standard deviation of the prediction errors σ from 0.35 to 0.24, are modeled as a function of the depth to the layer at which the shear-wave velocity is 1400 m/s for G_d and the average shear-wave velocity up to a depth of 30 m for G_s. The parameters required for these additional corrections can be obtained from the nationwide shear-wave velocity structure models provided by the Japan Seismic Hazard Information Station (2019); these models include a 1000-m-grid deep structure model and a 250-m-grid shallow structure model.

2.2.3 Seismic fragility model

The property damage states of buildings as a result of ground shaking are evaluated using empirical seismic fragility functions, which describe the statistical relationships between the probability of exceeding a specified damage state and a ground motion intensity measure for past large earthquakes. Three seismic fragility functions for Japanese low-rise wooden buildings were selected from the existing functions. These are (1) the function derived from building damage data for the 1995 Kobe earthquake (Yamaguchi and Yamazaki 2001), (2) the function derived from building damage data for seven large earthquakes that occurred between 2003 and 2008 (Midorikawa et al. 2011), and (3) the function derived from building damage data for the 2011 Tohoku earthquake (Wu et al. 2016). These equations adopt the cumulative distribution function of a standard normal distribution as a statistical model when the JMA seismic intensity is used as an explanatory variable and compute the probability of exceeding a certain damage state ds:

$$p(DS \geq ds) = \Phi\left(\frac{I_{JMA} - \lambda}{\xi}\right), \tag{8}$$

where λ is the mean (i.e., the value of the JMA seismic intensity corresponding to a 50% probability) and ξ is the standard deviation.

The property damage states considered are (1) completely destroyed and (2) half-destroyed (note that these states may be termed differently depending on the literature), and their corresponding loss ratios to the total replacement cost are randomly assigned from 0.5 to 1.0 and from 0.2 to 0.5, respectively, in accordance with the Japanese post-disaster building damage assessment guideline (Cabinet Office, Government of Japan 2013). Note that, the partially destroyed damage state is not considered because Midorikawa et al. (2011) did not develop their function including its damage state and the function by Wu et al. (2016) does not fit the data well when including this damage state. Figure 2 compares the probability of exceeding the damage state for the three selected functions. There are non-negligible differences between the functions. In particular, the function derived from the building damage data for the Tohoku earthquake appears to compute a much lower probability of exceeding the completely destroyed state than the other functions. This may be related to differences in the ground motion period characteristics of the earthquakes. To consider the effects of the differences in the functions (i.e., the epistemic uncertainty) on the final risk assessment, the three functions were equally used in the Monte Carlo simulations.

Fig. 2 Comparison of the probability of exceeding the damage state for empirical seismic fragility functions of Japanese low-rise wooden buildings derived from building damage data from different earthquakes
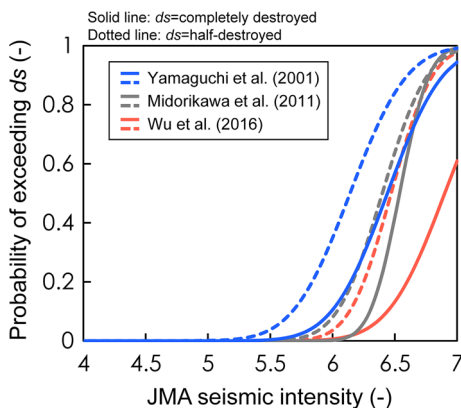
2.2.4 Post-earthquake ignition model

The post-earthquake ignition probability is evaluated for individual buildings using empirical post-earthquake ignition prediction equations, which are regression models derived from the fire records of past large earthquakes. Potential ignition sources inside buildings, such as electrical appliances, electrical wiring, and gas appliances, can be tipped over or damaged as a result of shaking and can come into contact with or heat nearby scattered combustible objects, resulting in ignition. Most existing equations therefore assume that the ground motion intensity is correlated with the ignition probability. For example, the equation developed by Nishino and Hokugo ([2020](#)), which is a Poisson regression model derived from the fire record of the Tohoku earthquake, computes the ignition probability per exposure population p_I in terms of the JMA seismic intensity:

$$p_I = \exp\left(\beta_0 + \beta_1 I_{JMA}\right), \tag{9}$$

where β_0 and β_1 are constants. This equation assumes that the probability of y ignition incidents occurring for n persons living in an area subjected to a seismic intensity of I_{JMA} can be approximated as a Poisson distribution and that the logarithm of its mean value μ can be modeled by a linear relation, where the logarithm of the exposure population n is treated as an offset term:

$$y \sim \text{Poisson}(\mu), \tag{10}$$

$$\ln \mu = \ln\left(n p_I\right) = \ln n + \beta_0 + \beta_1 I_{JMA}. \tag{11}$$

Note that the probability per population p_I needs to be converted into the probability per building to stochastically determine the origin buildings of the fires; this conversion can be done individually for each square grid cell with a specified size by multiplying the probability per population p_I by the ratio of the population to the number of buildings existing in the cell. However, the applicability of the regression model to different large earthquakes has not been examined.

Regression analyses were therefore conducted for three recent major large earthquakes in Japan, i.e., the Kobe earthquake, the Tohoku earthquake, and the Kumamoto earthquake, to explore the differences in the post-earthquake ignition prediction equations for

these earthquakes. Building fires that occurred as a result of ground shaking up to 72 h after the earthquakes were extracted from the fire records for the three earthquakes (Japan Association for Fire Science and Engineering 2016; Suzuki and Matsubara 1995; Suzuki and Shinohara 2017); the extracted information included the fire locations (addresses), dates and times of occurrence, ignition sources, and dates and times of fire brigade detection. Figure 3 overlays the locations of the fires subject to analysis on the estimated JMA seismic intensity maps. There were 176 fires associated with the Kobe earthquake, 114 fires associated with the Tohoku earthquake, and 12 fires associated with the Kumamoto earthquake (4 with the foreshock and 8 with the mainshock). The estimated JMA seismic intensity map for the Kobe earthquake is based on the method proposed by Yamaguchi and Yamazaki (2001), which calculates the intensity backward from the building damage ratios for each district using empirical seismic fragility functions based on damage data in the vicinity of seismic stations. The maps for the Tohoku earthquake and the Kumamoto earthquake are based on QuiQuake (National Institute of Advanced Industrial Science and Technology 2013), which is a national earthquake map estimation system based on records observed by nationwide strong-motion seismograph networks operated by the National Research Institute for Earth Science and Disaster Prevention of Japan. The equations were developed individually for each earthquake following the procedures adopted by Nishino and Hokugo (2020). The procedures are as follows. (1) The number of ignition incidents is
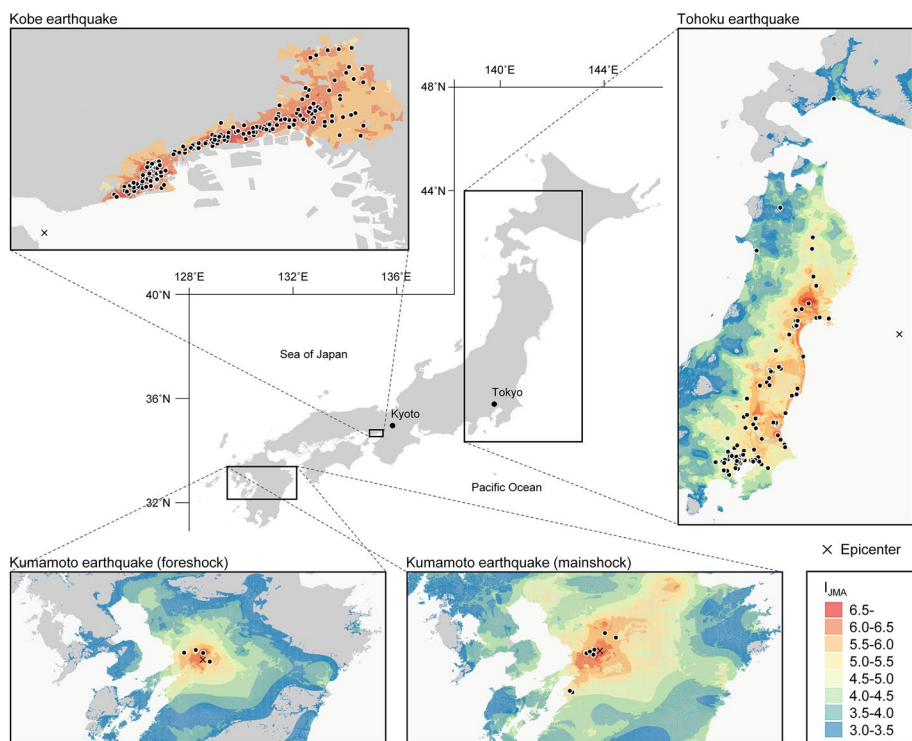
Fig. 3 Locations of building fires that occurred as a result of ground shaking up to 72 h after three recent major large earthquakes in Japan and their estimated Japan Meteorological Agency (JMA) seismic intensity maps. There were 176 fires linked to the 1995 Kobe earthquake, 114 fires linked to the 2011 Tohoku earthquake, and 12 fires linked to the 2016 Kumamoto earthquake

counted for each specified JMA seismic intensity interval by overlaying the locations of the ignition incidents on the estimated JMA seismic intensity map. (2) The exposure population is counted for each specified JMA seismic intensity interval by overlaying grid census data on the estimated JMA seismic intensity map. (3) A Poisson regression is conducted for the dataset of the number of ignition incidents versus the median value of each specified JMA seismic intensity interval, and the values of the model parameters are determined using the maximum likelihood estimation. Figure 4 compares the ignition probability per exposure population for the three developed equations. Note that the data points marked by dots, which are plotted to visually confirm the goodness of fit to the data, represent the ratios of the number of ignition incidents to the exposure population for each specified JMA seismic intensity interval and, therefore, no data points are plotted for intervals in which the number of ignition incidents or the exposure population was zero. For the Kumamoto earthquake, the data points are plotted separately for the foreshock (marked with a cross) and the mainshock (marked with a plus), but the equation was developed without distinguishing between them. The values of β_0 and β_1 were estimated to be -23.335 and 2.239, respectively, for the Kobe earthquake, -20.209 and 1.413, respectively, for the Tohoku earthquake, and -21.705 and 1.749, respectively, for the Kumamoto earthquake. There are non-negligible differences between the equations. In particular, the equation for the Kobe earthquake appears to compute much higher ignition probabilities than the other two equations. Even though seismic gas shutoff systems for household use have been widely prevalent in Japan since the Kobe earthquake (the installation rate has increased from 75% at the time of the Kobe earthquake to nearly 100% in recent years) and this measure could have been successful in reducing post-earthquake ignition incidents since then, the large differences in the ignition probability do not appear to be explained by ignition prevention measures alone. Differences in the ground motion period characteristics and resulting building damage severities for the different earthquakes could significantly contribute to the differences between the equations, as opposed to differences in the installation rate of ignition prevention measures. To consider the effects of the differences in the ignition models (i.e., the epistemic uncertainty) on the final risk assessment, the three post-earthquake ignition prediction equations were equally used in the Monte Carlo simulations. Note that all post-earthquake ignition incidents are assumed to occur simultaneously soon after an earthquake when simulating the urban fire spread because the ignition incidents, which may vary in their initiation time, are primarily concentrated in the period soon after the earthquake occurs (e.g., Nishino and Hokugo 2020).

Fig. 4 Comparison of the ignition probability per exposure population for the empirical post-earthquake ignition prediction equations derived from fire records from different earthquakes
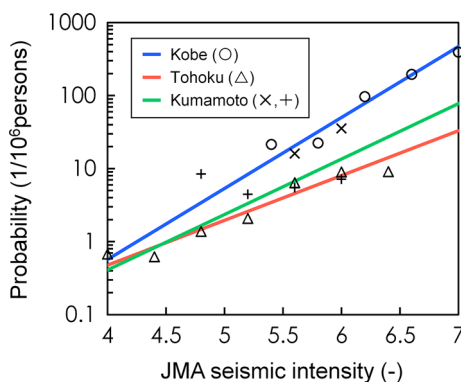
Even if a combustible object inside a room is ignited, a fire can burn out without spreading to adjacent combustible objects or may be extinguished by occupants during its initial stages. The latter effect of potential occupant firefighting is considered when determining the origin buildings of fires because little information is available concerning the self-extinguished fires. Introducing the probability p_E that an ignition incident inside a building is extinguished by the building occupants during its initial stages, the probability p_O that an ignition incident inside a building will develop into a fire involving the entire building can be written as

$$p_O = p_I(1 - p_E) \tag{12}$$

Equation (12) enables a stochastic determination of the buildings from which fires originate using random numbers, which are then used as inputs in the urban fire spread simulations. Note that p_I in Eq. (12) is the converted ignition probability per building. Whether occupants attempt firefighting and are successful in extinguishing fires may depend on the building damage and the regional damage situation resulting from the ground shaking; further, p_E may be correlated with ground motion intensity measures. However, there are few data available concerning such a model. Therefore, p_E is assumed to be constant regardless of the situation, with a value of 0.204, which corresponds the only such information currently reported in the literature: the ratio of the fires against which occupant firefighting was effective to all of the fires following the Kobe earthquake (Architectural Institute of Japan 1998). Given that the fires following the Kobe earthquake were concentrated in areas subjected to JMA seismic intensities of 6–7, this is a conservative assumption made to avoid underestimating losses resulting from post-earthquake fires; that is, p_E is expected to be higher when regions are subjected to smaller seismic intensities.

2.2.5 Weather model

The weather parameters required for urban fire spread simulations, which include the outdoor air temperature and the wind velocity and direction, are evaluated using reliable weather information specific to the region because urban weather can vary greatly depending on the region. The air temperature variation over time is very small compared to the gas temperature in building fires and hardly influences the urban fire spreading behavior. However, the wind variation over time significantly influences the fire spreading behavior. For example, the wind velocity and direction govern the inclined angle and extension direction of window-ejected flames and fire plumes and the flying distance and direction of firebrands released from burning buildings. One-year weather observation paired data were adopted as reliable information containing the hourly recorded weather parameters at a given meteorological station (i.e., 8760 h of paired data). Time histories of the weather parameters for a given time period were sampled from the data of the station closest to the region subject to analysis by randomly specifying the month, day, and hour of the earthquake occurrence; that is, the weather parameters change over time throughout the urban fire spread simulations. This manner of sampling reflects the actual weather trends in Monte Carlo simulations; simply put, the actual observed frequency of calm or windy days is reflected in the simulations. Note that the air humidity, which could influence the fire spread rate, is not considered because it is not incorporated in the adopted urban fire spread model (described in Sect. 2.2.6).

2.2.6 Urban fire spread model

Damage to buildings as a result of post-earthquake fires is evaluated using a dynamic urban fire spread model, which predicts the buildings involved in fires as a function of time. The physics-based urban fire spread model developed by Nishino (2019) was selected from the existing models because it explicitly formulates the mechanisms of the urban fire spread using physical knowledge in the field of fire safety engineering and its performance has been validated by simulating past great urban fires in Japan and comparing the simulations with fire reports. To simulate realistic urban fire spreading behavior following earthquakes, the model, which is for urban fires during normal times, is further extended to include the effects of structural damage resulting from ground shaking and water spray by firefighters. While the effects of water spray by firefighters are incorporated into the governing equations of the existing model, the effects of structural damage resulting from ground shaking are treated as additional corrections depending on the structural damage states. The structural damage states considered are collapsed, heavily damaged, and moderately damaged and are assigned to individual buildings considering their statistical correlation with the pre-evaluated property damage states (Miyakoshi et al. 2000).

Figure 5 illustrates a schematic of the implemented post-earthquake urban fire spread model. The model simulates the behavior of individual building fires under the influence of neighboring building fires and therefore is primarily composed of two sub-models, that is, the building fire sub-model for predicting the physical quantities of fires inside buildings and the building-to-building fire spread sub-model for predicting the ignition of neighboring buildings as a result of heat transfer from burning buildings.

The building fire sub-model is based on one-layer zone modeling. The one-layer zone modeling assumes a room in a building as a control volume, in which the gas properties are uniform regardless of the spatial location, and predicts physical quantities, such as the gas temperature, as a function of time by simultaneously solving the governing equations for the conservation of mass, energy, and mass fraction of chemical species (oxygen o and gasified fuel f) and the gas state, which are formulated for each control volume. Note that it is typically difficult to know the individual room layouts for each building at a regional
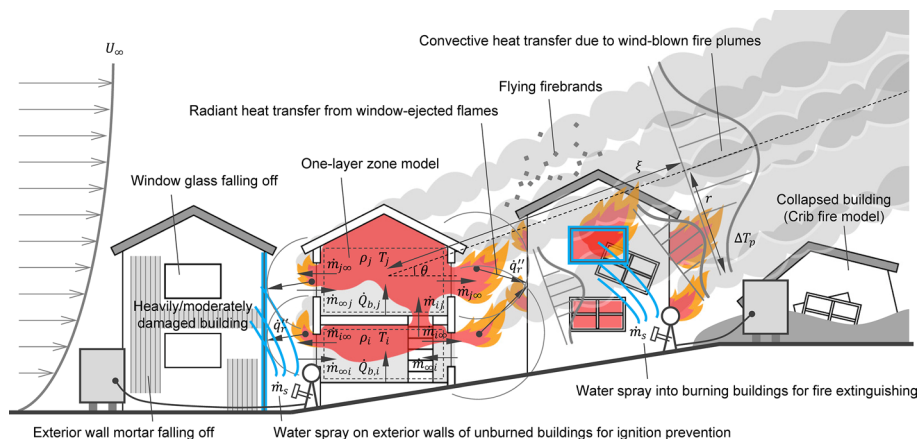

Fig. 5 Schematic of a physics-based post-earthquake urban fire spread model including the effects of structural damage resulting from ground shaking and water spray by firefighters

scale, and therefore, a control volume is set for each floor in this study neglecting partition walls. The governing equations for the i-th control volume are given as

$$\frac{\partial(\rho_i V_i)}{\partial t} = \dot{m}_{b,i} + \sum_j \left(\dot{m}_{ji} - \dot{m}_{ij} \right) + \dot{m}_{v,i}, \tag{13}$$

$$\frac{\partial(c_p \rho_i V_i T_i)}{\partial t} = \dot{Q}_{b,i} + c_p \dot{m}_{b,i} T_p + \sum_j \left(c_p \dot{m}_{ji} T_j - c_p \dot{m}_{ij} T_i \right) - \dot{Q}_{L,i} - L_v \dot{m}_{v,i} + c_p \dot{m}_{v,i} T_v, \tag{14}$$

$$\frac{\partial(Y_{X,i} \rho_i V_i)}{\partial t} = \dot{\Gamma}_{X,i} + \sum_j \left(Y_{X,j} \dot{m}_{ji} - Y_{X,i} \dot{m}_{ij} \right), \tag{15}$$

$$\rho_i V_i = \rho_j V_j \approx 353, \tag{16}$$

where j denotes the control volume (or outdoor space) adjacent to the i-th control volume, ρ is the gas density, V is the gas volume, c_p is the specific heat at constant pressure, T is the gas temperature, T_p is the pyrolysis temperature of combustible objects, T_v is the vaporization temperature of water, $\dot{m}_b$ is the mass loss rate of combustible objects, $\dot{m}_{ij}$ is the mass flow rate through openings from the i-th control volume to the j-th control volume, $\dot{m}_v$ is the production rate of water vapor, $\dot{Q}_b$ is the heat release rate resulting from combustion, $\dot{Q}_L$ is the total heat loss rate to the boundary walls, opening members, and adjacent spaces through openings, L_v is the latent heat of vaporization of water, Y_X is the mass fraction of the chemical species X, $\dot{\Gamma}_X$ is the production rate of the chemical species X, and t is time. Equations (13)–(16) enable the fire suppression effect of water sprayed into burning buildings by firefighters to be considered by determining the production rate of water vapor $\dot{m}_v$ from the water flow rate from a fire hose nozzle, which is typically up to 470 L/min. The boundary wall temperature is predicted by solving a one-dimensional heat conduction equation in the thickness direction using the finite difference method.

Equations (13)–(16) are applied to buildings that maintain their original compartments following an earthquake (i.e., all buildings except collapsed buildings). Conversely, not much information is available concerning the modeling of the fire behavior of collapsed buildings, which may be different from that of compartmented buildings. Given that numerous broken pieces of buildings are piled up, the fire behavior of collapsed buildings can be similar to that of wood cribs, which are made by arranging wood sticks in parallel crosses and are usually used in fire experiments to imitate actual combustible objects. Based on this assumption, equations for predicting the mass loss rate of wood cribs as a function of time (Babrauskas 2002) were applied to collapsed buildings instead of the one-layer zone model.

The building-to-building fire spread sub-model treats the following mechanisms as contributing factors to the ignition of neighboring buildings: (1) the heat transfer by radiation from window-ejected flames and compartment gases, (2) the heat transfer by convection from wind-blown fire plumes, and (3) firebrands flying downwind from burning buildings. The ignition of neighboring buildings, which is caused by the combined effect of the above factors, is assumed to occur when one of the following conditions is met. (A) The cumulative net incident heat flux to combustible exterior walls or combustible objects inside the buildings resulting from flame radiation and plume

convection exceeds a critical value. (B) Firebrands fall onto combustible objects and ignite them without being extinguished. While the former condition is deterministically formulated, the latter condition is probabilistically formulated because the occurrence of spot fires as a result of firebrands has high uncertainty. These conditions are given as follows for buildings with combustible exterior walls:

$$\int_0^t \left[\varepsilon \dot{q}_{ex}'' - \left\{c_w w_{ex}(T_v - T_0) + w_{ex}L_v\right\} - h(T_{ig} - T_\infty)\right]^2 dt \geq \left[\frac{\sqrt{k\rho c}(T_{ig} - T_0)}{1.18}\right]^2, \tag{17}$$

$$p_S(t, t + \Delta t) = 1 - \prod_{k=1}^{M(t,t+\Delta t)} \left[1 - \beta\left(\int_t^{t+\Delta t} \dot{Q}_{b,k} dt\right)\left(\iint f(x)f(y)dxdy\right)\right] \geq \zeta, \tag{18}$$

where $\dot{q}_{ex}''$ is the incident radiative heat flux to the exterior walls from window-ejected flames and compartment gases, w_{ex} is the mass of water delivered onto the exterior walls per unit surface area per unit time (the water delivered density), c_w is the specific heat of water, T_0 is the initial water temperature, T_∞ is the ambient temperature including the temperature increase as a result of wind-blown fire plumes, T_{ig} is the ignition temperature of the exterior wall materials, ε is the emissivity of the exterior wall materials, $\sqrt{k\rho c}$ is the heat inertia of the exterior wall materials, h is the convective heat transfer coefficient, Δt is the time increment, $p_S(t, t + \Delta t)$ is the probability of a spot fire occurring in a given building as a result of firebrands in the interval $(t, t + \Delta t)$, $M(t, t + \Delta t)$ is the number of burning buildings in the interval $(t, t + \Delta t)$, $\dot{Q}_{b,k}$ is the heat release rate for the k-th burning building, $f(x)$ and $f(y)$ are the probability density functions of the firebrand travel distances in the wind direction and in the direction normal to the wind direction, respectively, β is a constant, which was identified as 5.0×10^{-9} in numerical reproductions of the Great Fire of Itoigawa in 2016 such that the model predictions for the number of spot fires and the fire spread rate were reasonably consistent with the fire report (Nishino 2019), and ζ is a uniform random number between 0 and 1. Equation (17) enables the ignition prevention effect of water sprayed on the exterior walls of neighboring unburned buildings by firefighters to be considered by determining the water delivered density w_{ex} from the water flow rate from a fire hose nozzle and the wall surface area. Equation (17) can also be applied to buildings with non-combustible exterior walls by using the incident radiative heat flux to inner combustible objects passing through opening members, even though a slight modification of the equation is required; however, Eq. (18) is not applied to buildings with non-combustible exterior walls.

Damage to wooden buildings as a result of ground shaking can enhance building-to-building fire spread. For example, the exterior walls of wooden buildings are sometimes covered with mortar in Japan to improve their fire resistance; however, the exterior wall mortar can fall off as a result of shaking, and therefore, hidden wooden members can be exposed following earthquakes. To consider this effect in urban fire spread simulations, wooden buildings for which the structural damage state is evaluated as collapsed, heavily damaged, or moderately damaged are treated as buildings with combustible exterior walls, even if their exterior walls were originally covered with mortar.

2.2.7 Fire brigade response model

Fire brigade responses to individual post-earthquake fire outbreaks can greatly influence the eventual regional fire damage. Realistic fire brigade responses are modeled here by dividing the response process into several stages, as shown in Fig. 6, that is, (1) fire brigades detect fire outbreaks and dispatch fire engines, (2) fire engines travel from fire stations to water sources, (3) firefighters extend hoses from water sources to fire control lines, and (4) firefighters determine targets and spray water using fire hose nozzles. While fire brigades typically respond to one fire in groups of several fire engines during normal times, such a response is not possible following large earthquakes because fire engines are forced to be dispatched to multiple fire outbreaks and the number of fire engines is limited. To describe realistic responses, the fire brigade response model assumes that one fire engine is dispatched to one fire outbreak; that is, if the number of fire outbreaks overwhelms the number of fire engines, some of the fires can spread without the influence of firefighting. The model also assumes that one fire hose nozzle is available per fire engine considering the typical role assignment of firefighters; that is, at least three firefighters typically ride in a single fire engine: One is the conductor, one is an operator that controls the pump, and one controls the fire hose nozzle and sprays the water. Only fire cisterns are treated as water sources available for firefighting because fire hydrants are less likely to be available after large earthquakes as a result of seismic damage to water pipelines (e.g., Gehl et al. 2021). In addition, based on road blockages resulting from building collapses following the Kobe earthquake (Imaizumi and Asami 2000), only roads with a width of 5.5 m or more are treated as travel routes for fire engines because narrow roads are less likely to be available following large earthquakes because of collapsed buildings and debris. These are conservative assumptions to avoid overestimating the effects of firefighting on the behavior of the urban fire spread (i.e., to avoid underestimating fire losses to buildings). Conversely, when firefighters extend their hoses, they are assumed to somehow be able to walk through even
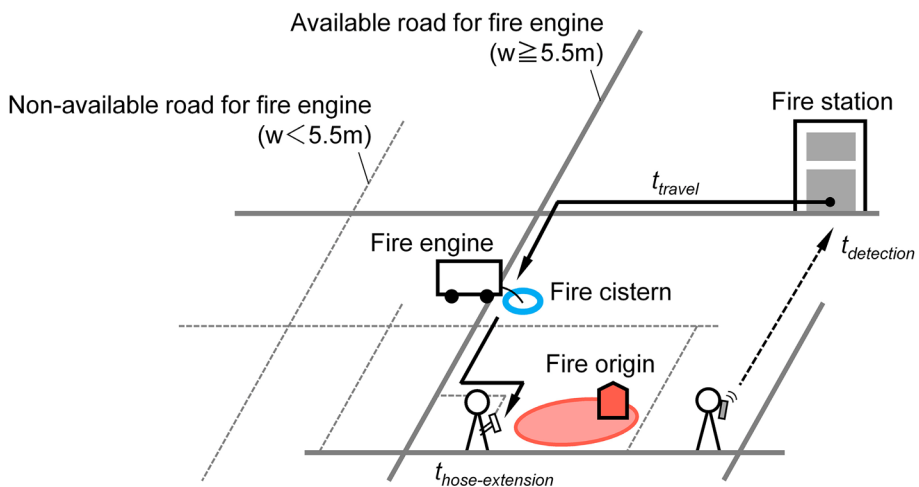

Fig. 6 Schematic of the modeled process of fire brigade responses to individual post-earthquake fire outbreaks: (1) fire brigades detect fire outbreaks and dispatch fire engines, (2) fire engines travel from fire stations to water sources, (3) firefighters extend hoses from water sources to fire control lines, and (4) firefighters determine targets and spray water using fire hose nozzles

narrow roads; that is, all roads are assumed to be available regardless of their width during
the hose extension stage.

When large fires occur in urban areas, firefighting typically focuses on preventing
the spread of fires to neighboring unburned buildings, rather than extinguishing burn-
ing buildings. In fact, it has been recommended that fire hose nozzles be preferentially
placed in highly likely fire spread directions (i.e., in the downwind and lateral direc-
tions) and the preliminary water spray be applied to the exterior walls of unburned
buildings to which fires are highly likely to spread to prevent the ignition of these build-
ings (Fire and Disaster Management Agency 2017a). The fire brigade response model
therefore defines the decision-making rules of the fire brigades on the basis of such
a principle to describe the realistic placement of fire engines with respect to water
sources and the realistic selection of targets for water spray. Accordingly, the effect of
preliminary water spray on the exterior walls of unburned buildings is considered in the
urban fire spread simulations, whereas water spray into burning buildings for fire extin-
guishing is neglected. As for the placement of the fire engines with respect to the water
sources, fire engines are assumed to travel to the nearest fire cistern to the fire outbreak
location given the fire cisterns that meet all of the following conditions: (a) fire cisterns
are next to wide roads (with a width of 5.5 m or more), (b) fire cisterns are downwind
of the fire outbreak location, (c) fire cisterns are not used by other fire engines, and (d)
the ambient temperature surrounding the fire cisterns is not too high as a result of fire
plumes that the firefighters cannot work. Note that when the wind velocity is less than
5 m/s, only conditions (a) and (c) apply. As for the targets for preliminary water spray,
which are automatically specified depending on the simulated fire spread situations,
firefighters are assumed to spray water on the exterior wall face subjected to the highest
radiative heat flux of the fires given the exterior wall faces that meet all of the follow-
ing conditions: (a) the exterior wall faces are downwind from the fire outbreak loca-
tion, (b) the exterior wall faces are facing the wind direction, (c) the exterior wall faces
are at a sufficient distance from neighboring buildings to deliver water to the faces, (d)
the exterior wall faces are within the reach of the water, which is assumed to be a dis-
tance of 400 m along roads from a fire cistern (note that the distance of 400 m corre-
sponds to a typical total extension distance of 20 hoses), (e) the exterior wall faces are
of unburned buildings, (f) the ambient temperature surrounding the exterior wall faces
is not too high as a result of fire plumes that the firefighters cannot work, (g) the exterior
wall faces are not targeted for water spray by other firefighters, and (h) the exterior wall
faces are subjected to more than a certain radiative heat flux from fires. Note that when
there are no exterior wall faces that meet all of the above conditions, the exterior wall
faces are searched again replacing condition (b) with the condition that the exterior wall
faces do not have their back to the wind direction. If there are still no exterior wall faces
that meet all of the conditions, the exterior wall faces are searched once again exclud-
ing conditions (a) and (b). These rules were determined by visually verifying the model
predictions for a hypothetical urban area with equal-size wooden buildings, as shown in
Fig. 7, where water sources are assumed to be located at 24 intersections. This verifica-
tion, which assumes that 10 fire engines arrive and specifies the arrival time individu-
ally for each fire engine, shows that the model can simulate realistic firefighting under
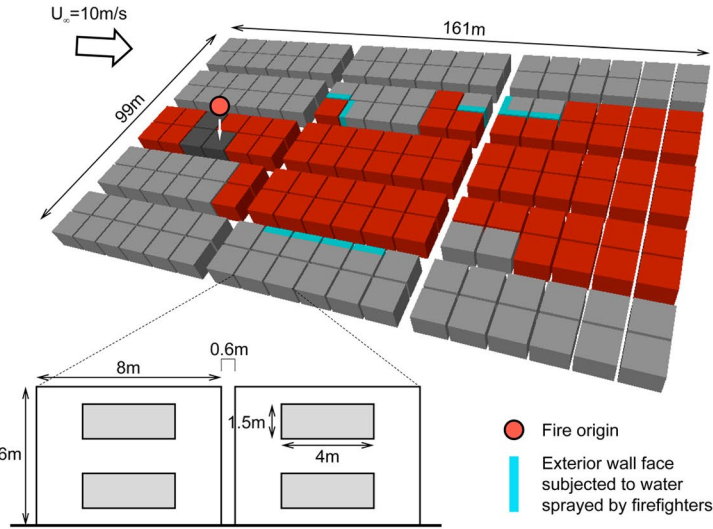
30 min after the outbreak

Spot fires
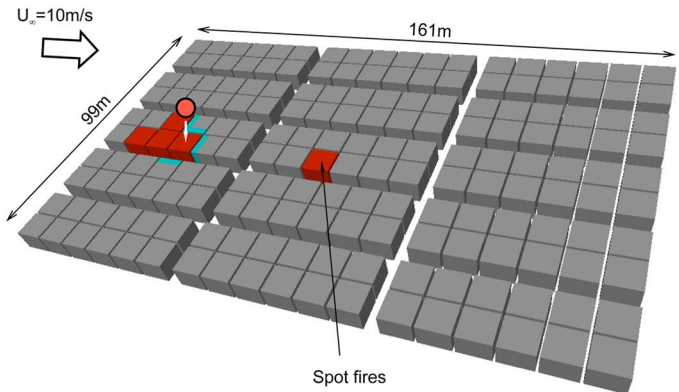
60 min after the outbreak
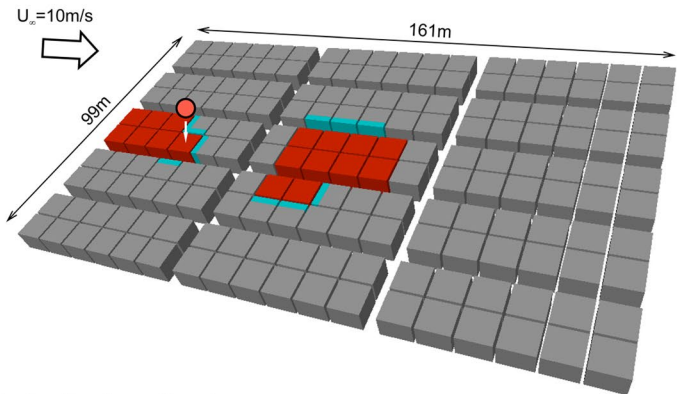
120 min after the outbreak

strong wind conditions (here, the wind velocity is 10 m/s) such that water is primarily sprayed to prevent downwind fire spreading, while the fires are localized. However, the firefighters are forced to change the water spray to prevent lateral fire spread after the fires are enlarged by spot fires because the firefighters cannot work in the downwind region as a result of wind-blown fire plumes. Consequently, fires increasingly spread in the downwind direction. This example represents a situation in which the fires overwhelm the firefighting capability as a result of spot fires; this is consistent with the situation of the 2016 Itoigawa Great Fire (Fire and Disaster Management Agency 2017b). The water flow rate from a fire hose nozzle is assumed to be constant, with 7.8 kg/s (i.e., 470 L/min) adopted as a typical value. Water spray from a fire hose nozzle is assumed to stop when the remaining amount of water in the fire cistern connected to the nozzle drops to zero.

Water spray is assumed to start at the earliest after the firefighters completely extend the hoses. The response time including the time to detection, $t_{response}$, is defined as the time to complete the hose extension and is evaluated individually for each fire outbreak as the sum of the time to detection $t_{detection}$, the travel time between a fire station and a water source t_{travel}, and the time required for hose extension $t_{hose - extension}$:

$$t_{response} = t_{detection} + t_{travel} + t_{hose - extension}. \tag{19}$$

The time to detection typically has high uncertainty and can be dominant in Eq. (19), while the travel time and the hose extension time can be deterministically evaluated from the distance and the velocity. Therefore, the time to detection needs to be treated as a random variable. Figure 8 shows the frequency distributions of the time from outbreak to detection for three recent major large earthquakes in Japan, i.e., the Kobe earthquake, the Tohoku earthquake, and the Kumamoto earthquake. As in Sect. 2.2.4, building fires that occurred as a result of ground shaking up to 72 h after the earthquakes were extracted from the fire records for the three earthquakes (Japan Association for Fire Science and Engineering 2016; Suzuki and Matsubara 1995; Suzuki and Shinohara 2017). Note that the sample sizes become smaller because of an additional extraction condition: the dates and times of the fire brigade detection are known. Even though the distribution for the Kumamoto earthquake is just a reference because the number of the fires was small, the time to detection after the earthquakes appears to vary greatly and is highly likely to become longer than that during normal times, as suggested by Sugii et al. (2008). This could be related to the fact that calls to fire brigades are typically jammed after earthquakes because of the many non-emergency calls unrelated to the earthquake, fires, or rescue. Focusing on JMA seismic intensities of 5.5 or more, the distributions appear to not differ much depending on the intensity intervals; that is, the distributions for an intensity of 5.5 or more are similar for the Kobe earthquake and the Tohoku earthquake. Even though the distributions for lower intensity events appear to be biased toward the left compared to those for an intensity of 5.5 or more, the entire distribution for the Kobe earthquake, for which the sample size appears to be sufficiently large, is used to stochastically generate the time to detection. This is a conservative assumption to avoid overestimating the effects of firefighting on the behavior of urban fire spread (i.e., to avoid underestimating fire losses to buildings). Conversely, the travel time is simply determined from the distance along the wide roads assuming a travel velocity of 10 km/h, which considers the possibility that the fire engines will need to move through traffic jams. The hose extension time is simply evaluated by dividing the maximum hose extension distance by a hose extension velocity of 2.6 m/s, a value based on actual measurements of firefighter performance (Tokyo Fire Department 1998).
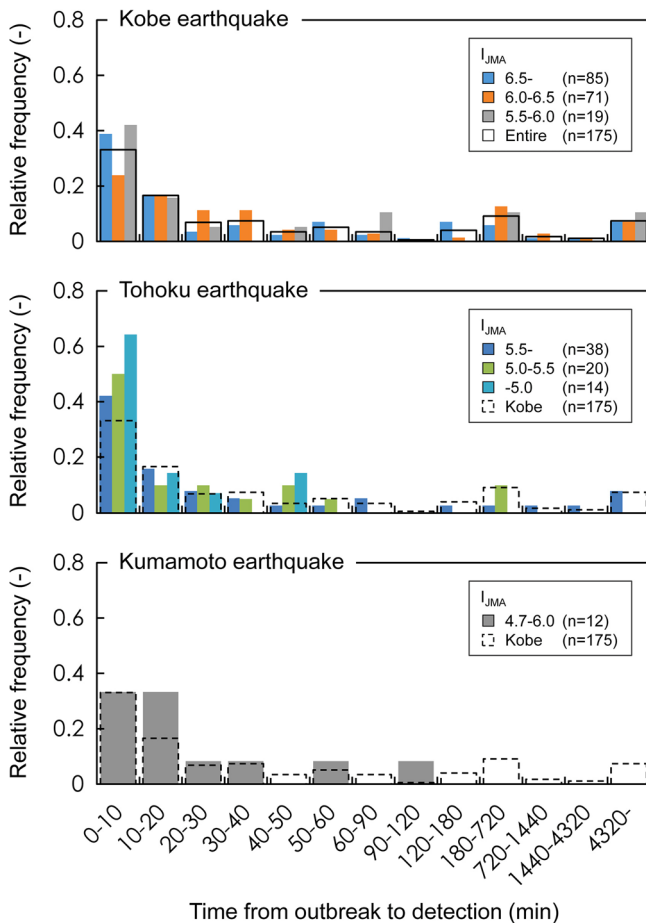
Fig. 8 Frequency distributions of the time from outbreak to detection for building fires that occurred as a result of ground shaking up to 72 h after three recent major large earthquakes in Japan. Note that the sample sizes are smaller than the actual number of fires because the dates and times of detection are not known for all fires

3 Application

3.1 Numerical setup

To illustrate an application of the proposed methodology, a realistic case study was conducted focusing on possible large earthquakes with specified source faults. Figure 9 shows the study area. A historical urban area of the Kamigyo Ward, Kyoto, was selected as the study area because it is one of the most densely built residential areas with old wooden buildings in Japan; of the various areas of Kyoto, it is also especially vulnerable to ground shaking and post-earthquake fires, and improving its safety is a serious priority of the local government. This area, which stretches 1.8 km from east to west and 2.6 km from north to south, is surrounded by very wide streets on all sides. Therefore, fires are not likely to
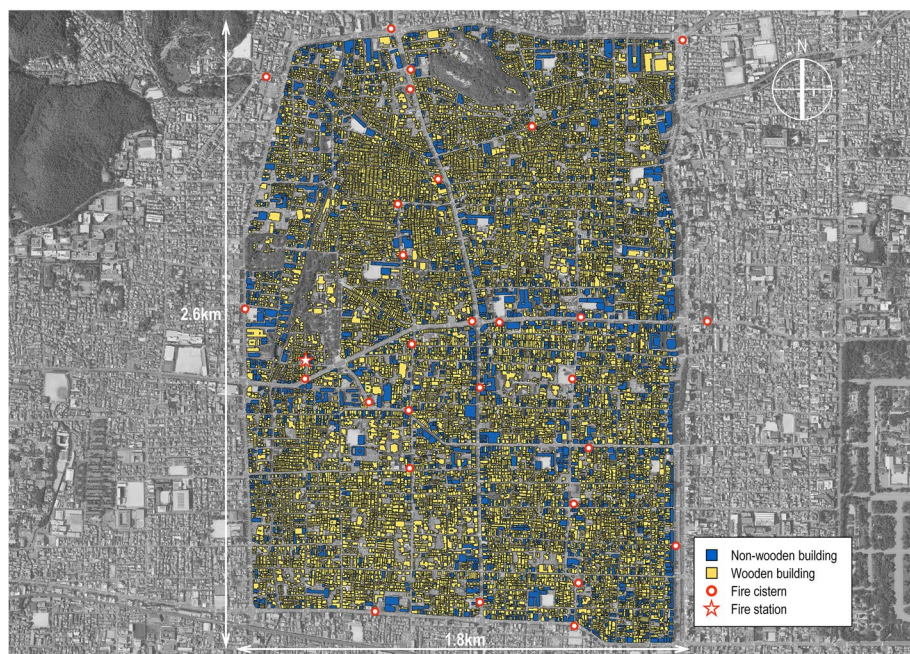
Fig. 9 Building exposure data for the study area provided by the Geospatial Information Authority of Japan and locations of fire stations and cisterns

spread across these streets. The used building exposure data were provided by the Geospatial Information Authority of Japan and contain information concerning the building locations, footprints, and construction types (wooden/non-wooden). According to these data, the study area is composed of 21,923 wooden buildings and 2802 non-wooden buildings. Because the above data do not include information concerning the building heights, the number of floors was assumed depending on the construction type; that is, the number of floors was assumed to be two for wooden buildings and three for non-wooden buildings. The thermal properties of the exterior walls, which greatly influence the behavior of the urban fire spread, were modeled as those of wood for wooden buildings and those of concrete for non-wooden buildings. Specific value settings for such building combustion properties, which include the mass density of the movable and fixed combustible objects, follow those of a previous study (Nishino 2019). Note that the wooden buildings in this case study were treated as wooden buildings without fire protection for the exterior walls and openings. The area of the exterior wall openings, which also greatly influences the behavior of the urban fire spread, was assumed because there are no data concerning the actual situation. In accordance with a previous study (Nishino 2019), the ratio of the opening area to the wall surface area was modeled as a function of the distance to the adjacent buildings. The unit replacement cost of the buildings, which is required for loss estimations, was determined from Kyoto building statistics to be 1732 USD/m^2 for wooden buildings and 3022 USD/m^2 for non-wooden buildings (note that the cost for non-wooden buildings was derived from statistics for reinforced concrete buildings). Summing the products of the unit replacement cost and the total floor area (i.e., the footprint area multiplied by the number of floors) for all the buildings, approximately 10,262 million USD was obtained as the total asset value of the study area. The settings for the fire brigades, such as the locations of the

fire stations and the number of fire engines, were based on the actual situation provided on the website of the municipal fire department; that is, there is only one fire station in the study area and it has two fire engines. Note that additional fire engines were not considered as being dispatched from other fire stations to this area because this would not be realistic in the event of multiple simultaneous post-earthquake fires. The locations of the fire cisterns were also based on the actual situation, given information previously reported in the literature (Matsumoto et al. 2021), while the amount of water stored in the fire cisterns was assumed to be uniform at 40 m^3, which is the minimum requirement prescribed by the Fire Service Act of Japan.

Table 1 lists the considered earthquakes and their activity model parameters. Six earthquakes along major active faults in the vicinity of the study area were selected from the earthquakes included in national seismic activity models for Japan (Morikawa and Fujiwara 2016) because they have specified source faults and can cause strong ground motion in the study area. For these earthquakes, the models specify a single magnitude and its probability of occurrence. Because the average life span of Japanese wooden houses is reported to be approximately 51 years as of 2005 (Komatsu 2008), a 50-year future time period was adopted when evaluating the earthquake occurrence probability and the loss exceedance probability. The fault location and geometry used in the ground shaking simulations were provided by the Japan Seismic Hazard Information Station (2019). Note that the shortest distance from the fault plane was determined by dividing the fault plane into multiple elements, calculating the distance from the center of each element, and then adopting the minimum. Figure 10 shows the mean value distribution of the JMA seismic intensity for each of the considered earthquakes representing the central tendency of the ground shaking simulations; this distribution was computed using the ground motion prediction equation adopted in this study (Morikawa and Fujiwara 2013). The overall distributions, which reflect the attenuation characteristics and the site amplifications, vary greatly depending on the earthquakes and demonstrate that the ground shaking simulations in this study can generate realistic distributions of the seismic intensity. Focusing on the study area, which is localized, the seismic intensity varied on average from approximately 5.0 to 6.0 depending on the earthquake.

To obtain reliable risk estimates, the number of trials for the Monte Carlo simulations needs to be sufficient. As the result of trial and error, 1800 trials were conducted individually for each of the considered earthquakes. Unlike the ground shaking simulations and the seismic damage predictions implemented in this study, the urban fire spread simulations need to

Table 1 Six earthquakes along major active faults and their activity model parameters (Morikawa and Fujiwara 2016)

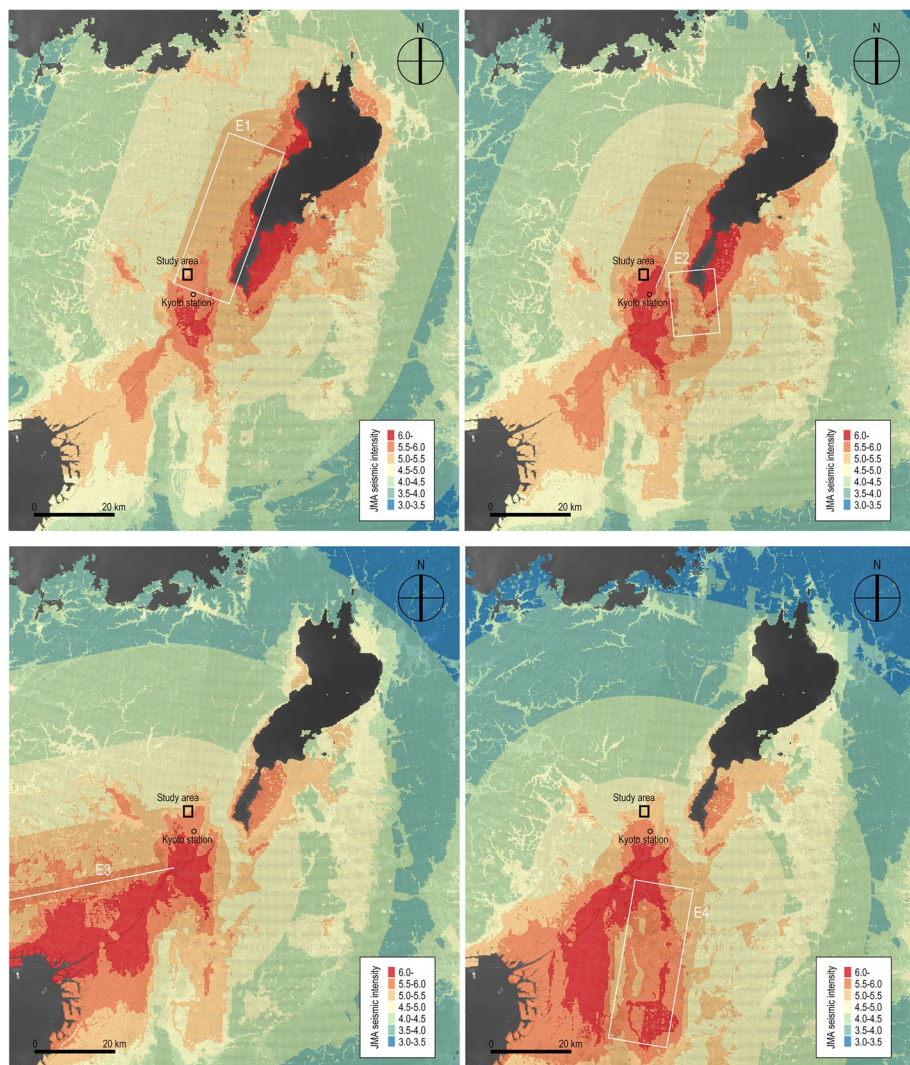| ID	Name of active fault	Moment magnitude	Mean recurrence interval (year)	Time of the latest event (years ago)	Probability of occurrence within 50 years (%)
E1	Biwako Seigan	6.9	4500	835	0.001
E2	Hanaore	6.9	4200	2800	0.952
E3	Arima-Takatsuki	7.1	1000	424	0.084
E4	Ikoma	6.9	3000	1620	0.272
E5	Kyoto Nishiyama	7.0	3500	2400	1.358
E6	Rokko-Awaji	7.3	900	520	2.158

Fig. 10 Specified source faults for the six earthquakes (Morikawa and Fujiwara 2016) and the distributions of the mean value of the JMA seismic intensity predicted by the ground motion prediction equation

specify the simulation period. A period of 72 h was adopted as the simulation period because urban fires are expected to die down, at the latest, approximately 72 h after an earthquake.

3.2 Results and discussion

3.2.1 Variability of the post-earthquake fire spread

Figure 11 shows examples of the post-earthquake urban fire spread simulations visualized using Google Earth, where three-dimensional objects colored in gray, red, and black
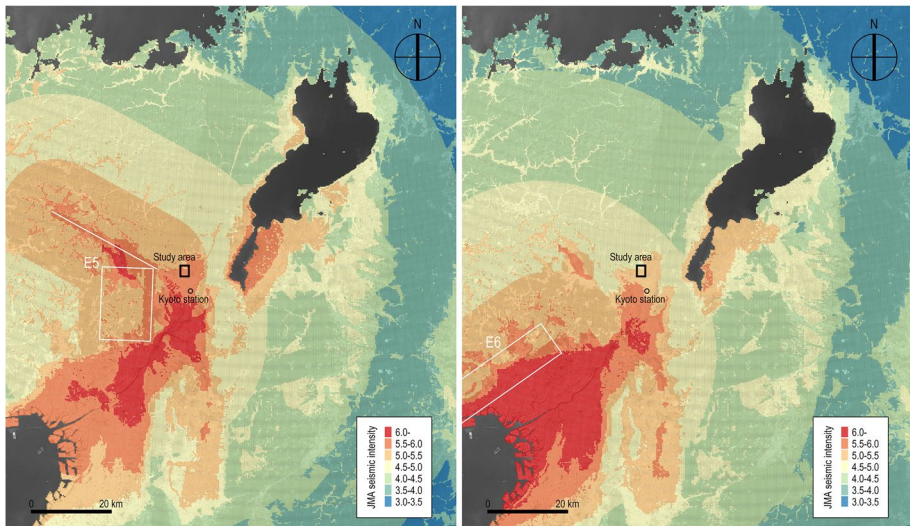
Fig. 10 (continued)

represent unburned buildings, burning buildings, and burned-out buildings, respectively. The simulations successfully describe realistic behaviors of the post-earthquake urban fire spread. To be specific, the fires simultaneously started from multiple buildings in very different locations and propagated to neighboring buildings one after another. While the fires enlarged the damaged areas, burning buildings began to burn out in sequence nearer the fire origins and therefore formed belt-like distributions along the fire fronts. As expected, the buildings involved with the fires varied greatly depending especially on the number and locations of the post-earthquake fire occurrences, which contributed to the complex behaviors of the fire spread combined with the time variation in the wind velocity and direction and the irregularity of the spatial distribution of the buildings.

Figure 12 shows the relationship between the eventual number of burned-out buildings and the number of fire occurrences for all post-earthquake fire scenarios predicted following the occurrence of the Hanaore earthquake. While non-fire-occurrence scenarios account for approximately 45% of all fire scenarios, the number of fire occurrences ranges up to eight and its cumulative frequency distribution is more right-skewed than typical Poisson distributions because different Poisson regression models for the post-earthquake fire ignition incidents were used in a mixture via the Monte Carlo simulations. The eventual number of burned-out buildings varies greatly even if the number of fire occurrences is the same, even though on average the number of burned-out buildings appears to increase with the number of fire occurrences. This great variation results from the combined effect of the several uncertainties considered in this study; that is, uncertainties in the locations of the fire occurrences, the wind velocity and direction, the time for firefighters to complete hose extension, and the structural damage resulting from ground shaking.

3.2.2 Loss exceedance curves

Figure 13 shows the conditional loss exceedance curves evaluated for each of the considered earthquakes (i.e., the probability that the total loss to the buildings exceeds a certain
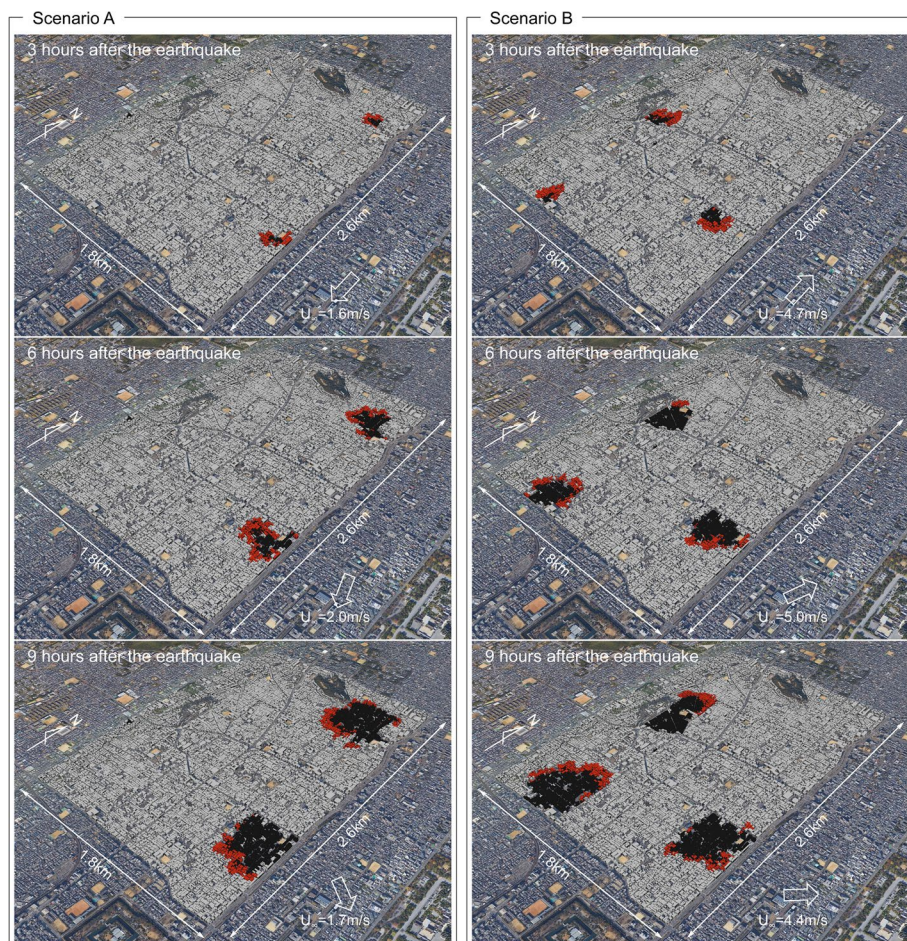
Fig. 11 Examples of the post-earthquake urban fire spread simulations visualized using Google Earth. The three-dimensional objects colored in gray, red, and black represent unburned buildings, burning buildings, and burned-out buildings, respectively

Fig. 12 Relationship between the eventual number of burned-out buildings and the number of fire occurrences predicted following the occurrence of the Hanaore earthquake
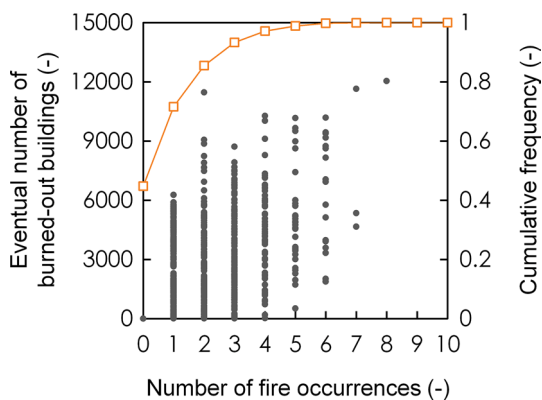
threshold when a given earthquake occurs). In this figure, lines colored in green represent the conditional loss exceedance curves considering the combined effect of ground shaking and post-earthquake fires, while lines colored in blue and red represent the conditional loss exceedance curves considering ground shaking alone and post-earthquake fires alone, respectively. The qualitative tendency found in common for all the earthquakes is that the curves for post-earthquake fires alone lie below the curves for ground shaking alone when the total loss is small. This relationship is reversed after the total loss becomes larger than a certain loss value. Therefore, at higher conditional exceedance probabilities, the curves for ground shaking alone dominantly contribute to the curves for the combined effect of ground shaking and post-earthquake fires. Conversely, at lower conditional exceedance probabilities, the curves for the post-earthquake fires alone dominantly contribute to the curves for the combined effect. This indicates that damage resulting from ground shaking occurs frequently following the occurrence of an earthquake but its impact to the total assets is limited. Conversely, damage resulting from post-earthquake fires occurs less frequently but may cause a devastating impact to the total assets. Note that the curves for ground shaking alone appear to form a step because different seismic fragility functions were used in a mixture via the Monte Carlo simulations and one function is significantly different from the others.

Figure 14 shows the loss exceedance curves evaluated using the above conditional loss exceedance curves and the earthquake occurrence probabilities (i.e., the probability that the total loss to the buildings exceeds a certain threshold at least once within 50 years when all the possible earthquakes are considered). In the same manner as in Fig. 13, the lines colored in blue, red, and green represent the loss exceedance curves considering ground shaking alone, post-earthquake fires alone, and their combined effect, respectively. As expected, the loss exceedance curves clearly reflect the qualitative tendency found in the
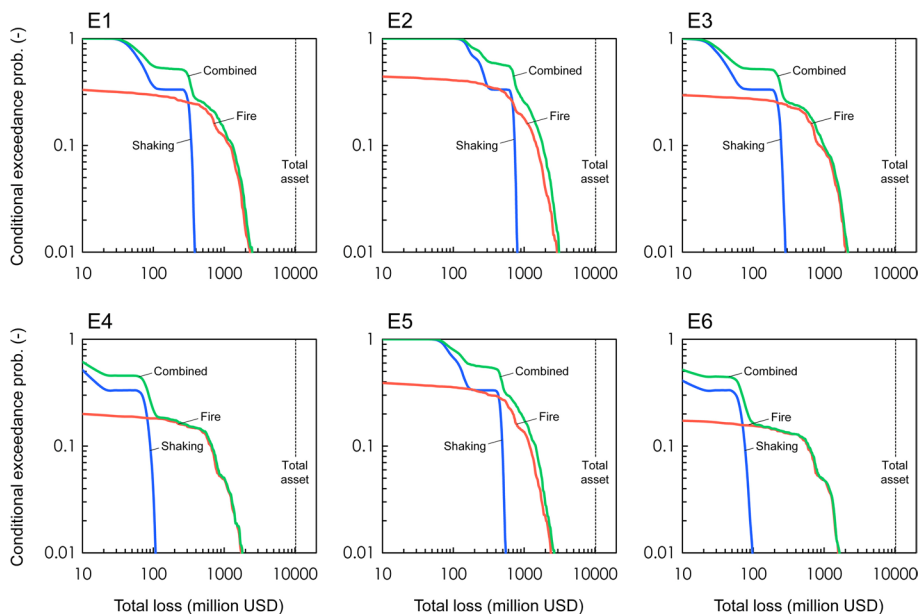

Fig. 13 Conditional loss exceedance curves evaluated for each of the considered earthquakes (i.e., the probability that the total loss to the buildings exceeds a certain threshold when a given earthquake occurs)

conditional loss exceedance curves; that is, as stated above, the loss exceedance curve for the combined effect of ground shaking and post-earthquake fires is dominantly affected by the curve for ground shaking alone at high exceedance probabilities and by the curve for post-earthquake fires alone at low exceedance probabilities and greatly depends on both curves at mid-exceedance probabilities. This result highlights a critical aspect of earthquake risk assessments for urban settlements; that is, conventional single-hazard risk assessments, which consider ground shaking alone, are likely to underestimate the loss exceedance probability and, in particular, miss the infrequent but devastating impact of post-earthquake fires on buildings. This indicates the importance of the proposed methodology for urban communities to more appropriately understand the inherent multi-hazard risk and make reasonable decisions for risk reduction objectives and options. The probabilities of the total loss exceeding 0.1%, 1%, and 10% of the total asset value (i.e., approximately 10, 100, and 1000 million USD) are approximately 3.6%, 2.5%, and 0.6%, respectively, over a 50-year period. Even though how these risk estimates are interpreted is up to urban communities, long-term measures typically used in Japan, such as joint or collaborative rebuilding and seismic or fire retrofitting, may be reasonable for the results in this study area given that the devastating impacts are infrequent. However, note that the results are limited to the area selected in this study; in particular, the individual contributions of the ground shaking and post-earthquake fires to the combined loss exceedance curve will vary depending on regional conditions, such as the density of old wooden buildings, the positional relationship of the region with respect to possible earthquake sources, and the magnitude and occurrence probability of earthquakes.

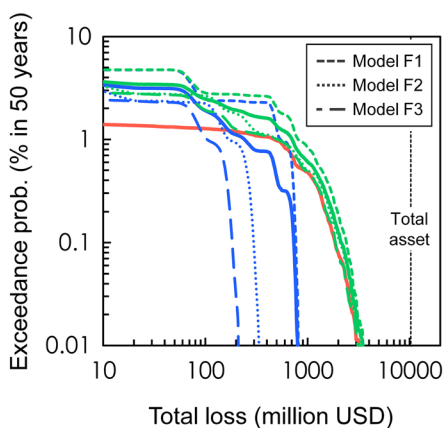### 3.2.3 Sensitivity to seismic fragility and post-earthquake ignition models

Figure 15 shows the sensitivity of the loss exceedance curves to the seismic fragility functions and the post-earthquake ignition prediction equations selected in this study. In the same manner as in Figs. 13 and 14, the lines colored in blue, red, and green represent the loss exceedance curves considering ground shaking alone, post-earthquake fires alone, and their combined effect, respectively. Dotted lines represent the loss exceedance curves evaluated using a single seismic fragility function or post-earthquake ignition prediction equation alone, while the solid lines represent the loss exceedance curves evaluated using a mixture of all of the fragility functions or ignition prediction

Fig. 14 Evaluated loss exceedance curves (i.e., the probability that the total loss to the buildings exceeds a certain threshold at least once within a 50-year period when all the possible earthquakes are considered)
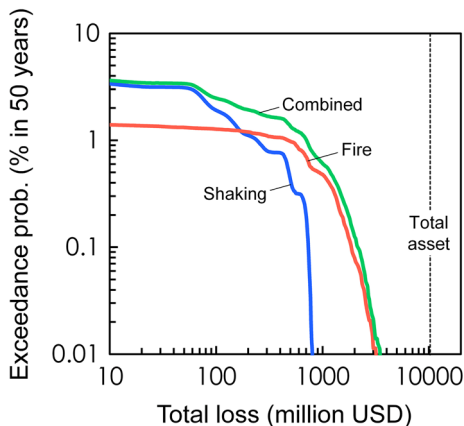
equations. For the seismic fragility functions, when the function based on the building damage data for the Kobe earthquake (Yamaguchi and Yamazaki 2001), referred to as model F1 in left panel of Fig. 15, is used alone, the loss exceedance curve for ground shaking alone is shifted to the right relative to the curve evaluated using the mixture of all of the functions. Conversely, when the other functions based on the building damage data after the Kobe earthquake (Midorikawa et al. 2011; Wu et al. 2016), referred to as models F2 and F3 in left panel of Fig. 15, are used alone, the loss exceedance curves for ground shaking alone are shifted to the left relative to the curve evaluated using the mixture of all of the functions. Corresponding to this, the loss exceedance curves for the combined effect of the ground shaking and post-earthquake fires also shift similarly depending on the functions used. Therefore, as pointed out by Goda and Risi (2018), the effects of using different seismic fragility functions on the risk estimates can be significant. The same applies to the post-earthquake ignition prediction equations. When the equation based on the fire records for the Kobe earthquake, referred to as model I1 in right panel of Fig. 15, is used alone, the loss exceedance curves both for the post-earthquake fires alone and for the combined effect are shifted to the right relative to the curve evaluated using the mixture of all of the equations. Conversely, when the other equations based on the fire records for the Tohoku and Kumamoto earthquakes, referred to as models I2 and I3 in the right panel of Fig. 15, are used alone, the loss exceedance curves both for the post-earthquake fires alone and for the combined effect are shifted to the left relative to the curve evaluated using the mixture of all of the equations. This indicates that the post-earthquake ignition prediction equations, in addition to the seismic fragility functions, need to be carefully selected to appropriately assess the multihazard risk because the effects of using different post-earthquake ignition models on the risk estimates can be significant.
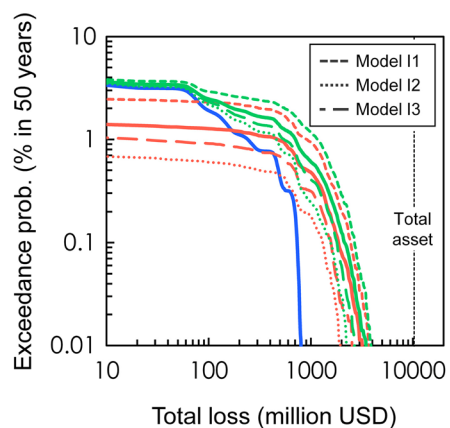

Fig. 15 Sensitivity of the loss exceedance curves to **a** the seismic fragility functions and **b** the post-earthquake ignition prediction equations selected in this study

4 Conclusions

A probabilistic methodology was proposed to assess the cascading multi-hazard risk for ground shaking and post-earthquake fires at a regional scale. The proposed methodology focuses on direct economic losses to buildings caused by the combined effect of ground shaking and post-earthquake fires and evaluates the exceedance probability of the regional shaking–fire losses in a predefined future time period by comprehensively considering various uncertainties via Monte Carlo simulations. The proposed methodology is an extension of a typical probabilistic seismic risk assessment and is built on national seismic activity models for Japan, which provide the fault location and geometry, magnitude, and occurrence probability for earthquakes with specified sources across Japan. To produce the multi-hazard shaking–fire risk assessments, post-earthquake fire damage prediction models were integrated with empirical ground motion prediction equations and seismic fragility functions. The fire damage prediction models were the following: (1) empirical post-earthquake ignition prediction equations that describe the ignition probability per exposure population as a function of the ground motion intensity, (2) an empirical weather model that randomly extracts time history samples for a given time period from hourly recorded weather data of the outdoor air temperature and the wind velocity and direction, (3) a physics-based urban fire spread model that describes the behavior of individual building fires considering building-to-building fire spread mechanisms, and (4) a fire brigade response model that automatically specifies targets for water spray depending on the simulated fire spread situations on the basis of predefined decision-making rules for the fire brigades. This integrated modeling enables a series of simulations of ground shaking, seismic damage, and post-earthquake urban fire spread for various scenarios and then converts the shaking–fire damage into losses according to the replacement costs. In particular, the post-earthquake urban fire spread simulations were performed on the basis of detailed building exposure data containing information concerning the building footprints, floors, and construction types for spatially distributed buildings treating the following factors as uncertain inputs: (a) the number and locations of the fire outbreaks, (b) the outdoor air temperature and the wind velocity and direction, (c) the time for firefighters to complete hose extension, and (d) the structural damage resulting from ground shaking.

To demonstrate the proposed methodology, a realistic case study was conducted for a historical urban area with closely spaced wooden buildings in Kyoto focusing on possible large earthquakes along major inland active faults. The results highlight the impact of multi-hazard consideration on risk assessments as opposed to conventional single-hazard approaches; that is, single-hazard risk assessments, which consider ground shaking alone, likely underestimate the loss exceedance probability and, in particular, miss the infrequent but devastating impact of post-earthquake fires on buildings. This indicates the importance of multi-hazard approaches and that the proposed methodology can serve as a tool to more appropriately understand the inherent multi-hazard risk and to promote the reasonable decision-making of urban communities for risk reduction. However, the influences of the epistemic uncertainty on the final risk assessments were not fully discussed in this paper, except that of the seismic fragility functions and post-earthquake ignition prediction equations. This aspect needs to be considered in future work. Even though the proposed methodology was developed for buildings in Japan, the methodology is flexible and there is room for improvement in the implemented models. Needless to say, they can be replaced with other suitable models depending on the given requirements. In particular, several fire models implemented in this study adopt conservative assumptions or treatments to avoid

underestimating post-earthquake fire losses. For example, the occupant firefighting probability during the initial stages, the time to detection of the fire brigades following an earthquake, and the post-earthquake availability of fire hydrants need to be modeled more appropriately in future work after collecting more data concerning actual situations during various earthquake events. Furthermore, the proposed methodology can be extended to include tsunami losses (i.e., a multi-hazard shaking–tsunami–fire risk assessment methodology) as a tool to support coastal communities that may be affected by offshore megathrust earthquakes along subduction zones. Although this study aimed to improve pre-earthquake decision-making in urban communities, the proposed methodology could also become a tool to support post-earthquake decision-making in disaster response organizations by extending it to post-earthquake rapid loss updating considering various field observations via Bayesian network modeling. These further improvements will contribute significantly to appropriate multi-hazard risk assessments and risk reduction.

Declarations

References

Architectural Institute of Japan (1998) Fire damage and civil activities. Damage to information systems. Report on the Hanshin-Awaji Earthquake Disaster (in Japanese)

Babrauskas V (2002) Heat release rates. In: The SFPE handbook of fire protection engineering, 3rd edn. National Fire Protection Association, Quincy

Baquedano Julia P, Ferreira TM, Rodrigues H (2021) Post-earthquake fire risk assessment of historic urban areas: a scenario-based analysis applied to the Historic City Centre of Leiria, Portugal. Int J Disaster Risk Reduct 60:102287

Cabinet Office, Government of Japan (2013) Guidelines for post-disaster building damage assessment (in Japanese). https://www.bousai.go.jp/taisaku/pdf/shishinall.pdf. Accessed 15 Apr 2022

Coar M, Sarreshtehdari A, Garlock M, Khorasani NE (2021) Methodology and challenges of fire following earthquake analysis: an urban community study considering water and transportation networks. Nat Hazards 109:1–31

Cousins J, Thomas G, Heron D, Smith W (2012) Probabilistic modeling of post-earthquake fire in Wellington, New Zealand. Earthq Spectra 28:553–571

Davidson RA (2009) Modeling postearthquake fire ignitions using generalized linear (mixed) models. J Infrastruct Syst 15:351–360

Dolce M, Prota A, Borzi B, Porto F, Lagomarsino S, Magenes G, Moroni C, Penna A, Polese M, Speranza E, Verderame GM, Zuccaro G (2021) Seismic risk assessment of residential buildings in Italy. Bull Earthq Eng 19:2999–3032

Earthquake Research Committee (2017) Strong ground motion prediction method for earthquakes with specified source faults ("Recipe"). The Headquarters for Earthquake Research Promotion. https://www.jishin.go.jp/main/chousa/17_yosokuchizu/recipe.pdf. Accessed 15 Apr 2022

Ellsworth WL, Matthews MV, Nadeau RM, Nishenko SP, Reasenberg PA, Simpson RW (1999) A physically based earthquake recurrence model for estimation of long-term earthquake probabilities. U.S. Geological Survey Open-File Report, pp 99–522

Fire and Disaster Management Agency (2006) Confirmed report on the Great Hanshin Earthquake. https://www.fdma.go.jp/disaster/info/assets/post1.pdf. Accessed 15 Apr 2022

Fire and Disaster Management Agency (2017a) Fire brigade response in strong winds. https://www.fdma.go.jp/laws/tutatsu/assets/291222_syo290.pdf. Accessed 15 Apr 2022

Fire and Disaster Management Agency (2017b) Report on how firefighting should be in the future based on the large-scale fire in Itoigawa City. https://www.fdma.go.jp/singi_kento/kento/items/kento209_15_houkokusyo.pdf. Accessed 15 Apr 2022

Gehl P, Matsushima S, Masuda S (2021) Investigation of damage to the water network of Uki City from the 2016 Kumamoto earthquake: derivation of damage functions and construction of infrastructure loss scenarios. Bull Earthq Eng 19:685–711

Goda K, Hong HP (2008) Estimation of seismic loss for spatially distributed buildings. Earthq Spectra 24:889–910

Goda K, Risi RD (2018) Multi-hazard loss estimation for shaking and tsunami using stochastic rupture sources. Int J Disaster Risk Reduct 28:539–554

Goda K, Risi RD, Luca FD, Muhammad A, Yasuda T, Mori N (2021) Multi-hazard earthquake-tsunami loss estimation of Kuroshio Town, Kochi Prefecture, Japan considering the Nankai-Tonankai megathrust rupture scenarios. Int J Disaster Risk Reduct 54:102050

Himoto K, Tanaka T (2008) Development and validation of a physics-based urban fire spread model. Fire Saf J 43:477–494

Imaizumi K, Asami Y (2000) A study on estimation of street-blockades caused by a great earthquake: to improve densely inhabited urban area for disaster prevention. J Arch Plan (trans AIJ) 65:225–231 (**in Japanese**)

Japan Association for Fire Science and Engineering (2016) Fires following the Great East Japan earthquake. Report on Fires Following the 2011 Great East Japan earthquake, Chapter 3, pp 1–36 (in Japanese)

Japan Seismic Hazard Information Station (J-SHIS) (2019) National Research Institute for Earth Science and Disaster Resilience. https://doi.org/10.17598/nied.0010

Kalakonas P, Silva V, Mouyiannou A, Rao A (2020) Exploring the impact of epistemic uncertainty on a regional probabilistic seismic risk assessment model. Nat Hazards 104:997–1020

Kappes MS, Keiler M, von Elverfeldt K, Glade T (2012) Challenges of analyzing multi-hazard risk: a review. Nat Hazards 64:1925–1958

Khorasani NE, Gernay T, Garlock M (2017) Data-driven probabilistic post-earthquake fire ignition model for a community. Fire Saf J 94:33–44

Komatsu Y (2008) Life time estimations of Japanese buildings and houses at the years of 1997 and 2005. J Arch Plan (trans AIJ) 73:2197–2205 (**in Japanese**)

Lee SW, Davidson RA (2010) Physics-based simulation model of post-earthquake fire spread. J Earthq Eng 14:670–687

Lee S, Davidson R, Ohnishi N, Scawthorn C (2008) Fire following earthquake—reviewing the state-of-the-art of modeling. Earthq Spectra 24:933–967

Marzocchi W, Garcia-Aristizabal A, Gasparini P, Mastellone ML, Ruocco AD (2012) Basic principles of multi-risk assessment: a case study in Italy. Nat Hazards 62:551–573

Matsumoto K, Okubo T, Kim D (2021) Study on water resources used against widespread fire after earthquakes and study on effective range of fire fighting activities at an earthquake: case study of traditional high-densited urban areas in Kamigyo-ku, Kyoto. J Disaster Mitig Hist Cities 15:113–120 (**in Japanese**)

Matsushima S (2020) Core-to-core collaborative research between Earthquake Research Institute, the University of Tokyo and Disaster Prevention Research Institute, Kyoto University during FY2014 to FY2018. J Disaster Res 15:187–201

Matthews MV, Ellsworth WL, Reasenberg PA (2002) A Brownian model for recurrent earthquakes. Bull Seismol Soc Am 92(6):2233–2250

Midorikawa S, Ito Y, Miura H (2011) Vulnerability functions of buildings based on damage survey data of earthquakes after the 1995 Kobe earthquake. J Jpn Assoc Earthq Eng 11:34–47 (**in Japanese**)

Mignan A, Wiemer S, Giardini D (2014) The quantification of low-probability–high-consequences events: part I. Gener Multi-Risk Approach Nat Hazards 73:1999–2022

Ming X, Xu W, Li Y, Du J, Liu B, Shi P (2015) Quantitative multi-hazard risk assessment with vulnerability surface and hazard joint return period. Stoch Env Res Risk Assess 29:35–44

Miyakoshi J, Hayashi Y, Fukuwa N (2000) Relationship between damage ranks with different criteria based on building damage. J Struct Eng B 46:121–134 (**in Japanese**)

Morikawa N, Fujiwara H (2013) A new ground motion prediction equation for Japan applicable up to M9 mega-earthquake. J Disaster Res 8:878–888

Morikawa N, Fujiwara H (2016) Updates to the seismic activity models of Japan: lessons from the Great Tohoku earthquake. Seismol Res Lett 87(6):1259–1264

National Institute of Advanced Industrial Science and Technology (2013) QuiQuake: quick estimation system for earthquake map triggered by observed records. https://gbank.gsj.jp/QuiQuake/index.en. html. Accessed 15 Apr 2022

Nishino T (2019) Physics-based urban fire spread simulation coupled with stochastic occurrence of spot fires. Stoch Env Res Risk Assess 33:451–463

Nishino T (2021) Probabilistic analysis of the vulnerability of fire departments to ignitions following megathrust earthquakes in the Nankai Trough subduction zone. Jpn Fire Saf J 120:103038

Nishino T, Hokugo A (2020) A stochastic model for time series prediction of the number of post-earthquake fire ignitions in buildings based on the ignition record for the 2011 Tohoku earthquake. Earthq Spectra 36:232–249

Nishino T, Tanaka T, Hokugo A (2012) An evaluation method for the urban post-earthquake fire risk considering multiple scenarios of fire spread and evacuation. Fire Saf J 54:167–180

Nishino T, Tanaka T, Tsuburaya S (2013) Development and validation of a potential-based model for city evacuation in post-earthquake fires. Earthq Spectra 29:911–936

Ogata K (1925) The Great Fire of Tokyo caused by the Great Kanto earthquake. Rep Imp Earthq Investig Comm 100:1–80 (**in Japanese**)

Omidvar B, Kivi HK (2016) Multi-hazard failure probability analysis of gas pipelines for earthquake shaking, ground failure and fire following earthquake. Nat Hazards 82:703–720

Sakai Y, Koyama S (2016) Knowledge on seismic response of buildings and damage. In: Earthquake ground motion and strong motion prediction: key items for learning the basics, 1st edn. Architectural Institute of Japan, pp 213–236 (in Japanese)

Scawthorn C (1986) Fire following earthquake. Fire Saf Sci 1:971–979

Scawthorn C (2011) Fire following earthquake aspects of the Southern San Andreas fault Mw 7.8 earthquake scenario. Earthq Spectra 27:419–441

Scawthorn C, O'Rourke TD, Blackburn FT (2006) The 1906 San Francisco earthquake and fire—enduring lessons for fire protection and water supply. Earthq Spectra 22:S135–S158

Scawthorn C, Cowell AD, Borden F (1996) Fire-related aspects of the Northridge earthquake. NIST GCR 98-743. Building and Fire Research Laboratory, National Institute of Standards and Technology, Gaithersburg

Schmidt J, Matcham I, Reese S, King A, Bell R, Henderson R, Smart G, Cousins J, Smith W, Heron D (2011) Quantitative multi-risk analysis for natural hazards: a framework for multi-risk modelling. Nat Hazards 58:1169–1192

Sekizawa A (1998) Post-earthquake fires and performance of firefighting activity in the early stage in the 1995 Great Hanshin-Awaji earthquake. In: IFAC Proceedings volumes, IFAC workshop on control in natural disasters (CND'98), Tokyo, Japan, 21–22 September, vol 31, pp 1–9

Selva J (2013) Long-term multi-risk assessment: statistical treatment of interaction among risks. Nat Hazards 67:701–722

Sugii K, Sekizawa A, Okabe H, Endo M, Zama S, Araiba K (2008) Necessity of structuring an effective scheme of acquiring disaster information by fire departments just after an earthquake. J Soc Saf Sci 10:89–96 (**in Japanese**)

Suzuki K, Matsubara Y (1995) Fires for 10 days after the 1995 Kobe earthquake. Rep Natl Res Inst Fire Disaster 49:21–30 (**in Japanese**)

Suzuki K, Shinohara M (2017) Summary of fires in the 2016 Kumamoto earthquake and countermeasures. Rep Natl Res Inst Fire Disaster 122:11–17 (**in Japanese**)

Thomas G, Heron D, Cousins J, Roiste M (2012) Modeling and estimating post-earthquake fire spread. Earthq Spectra 28:795–810

Tokyo Fire Department (1998) Standard action time of fire brigades. Report on firefighting measures in large buildings and special buildings, Chapter 3, pp 51–102 (in Japanese)

Wu H, Masaki K, Irikura K, Kurahashi S (2016) Empirical fragility curves of buildings in northern Miyagi Prefecture during the 2011 off the Pacific coast of Tohoku earthquake. J Disaster Res 11:1253–1270

Yamaguchi N, Yamazaki F (2001) Estimation of strong motion distribution in the 1995 Kobe earthquake based on building damage data. Earthq Eng Struct Dyn 30:787–801

Zhao S (2010) GisFFE—an integrated software system for the dynamic simulation of fires following an earthquake based on GIS. Fire Saf J 45:83–97